# Epistatic interactions between *PHOTOPERIOD-1, CONSTANS 1* and *CONSTANS 2* modulate the photoperiodic response in wheat

Lindsay M. Shaw[1, 2]*, Chengxia Li[1, 3]*, Daniel P. Woods[1, 3]*, Maria Alejandra Alvarez[1]*, Huiqiong Lin[1, 3], Mei Yee Lau[1], Andrew Chen[1, 4], and Jorge Dubcovsky[1, 3#]

*The first four authors contributed equally to this work

[1] Dept. Plant Sciences, University of California, Davis, CA 95616. U.S.A.

[2] Currently at Queensland Alliance for Agriculture and Food Innovation, The University of Queensland, Brisbane, QLD 4072, Australia

[3] Howard Hughes Medical Institute, Chevy Chase, MD 20815, U.S.A.

[4] Currently at School of Agriculture and Food Science, The University of Queensland, St Lucia, QLD, 4067, Australia.

Daniel P. Woods: ORCID 0000-0002-1498-5707
Jorge Dubcovsky: ORCID 0000-0002-7571-4345

**Short title:** Regulation of wheat heading time by photoperiod

**# Corresponding authors:** Jorge Dubcovsky, Email: jdubcovsky@ucdavis.edu, Phone: 530 (752)-5159.

**Abstract**

In Arabidopsis, *CONSTANS* (*CO*) integrates light and circadian clock signals to promote flowering under long days (LD). In the grasses, a duplication generated two paralogs designated as *CONSTANS 1* (*CO1*) and *CONSTANS 2* (*CO2*). Here we show that in tetraploid wheat plants grown under LD, combined loss-of-function mutations in the A and B-genome homeologs of *CO1* and *CO2* (*co1 co2*) result in a small (3 d) but significant ($P$<0.0001) acceleration of heading time both in *PHOTOPERIOD1* (*PPD1*) sensitive (*Ppd-A1b*) and insensitive (*Ppd-A1a*) backgrounds. Under short days (SD), *co1 co2* mutants headed 13 d earlier than the wild type ($P$<0.0001) in the presence of *Ppd-A1a*. However, in the presence of *Ppd-A1b*, spikes from both genotypes failed to emerge by 180 d. These results indicate that *CO1* and *CO2* operate mainly as weak heading time repressors in both LD and SD. By contrast, in the absence of functional *PPD1* alleles (*ppd1*), *Co1* accelerated heading time >60 d relative to *co1* under LD. We detected significant genetic interactions among *CO1*, *CO2* and *PPD1* alleles on heading time, which were reflected in complex interactions among these genes at the transcriptional and protein levels. Loss-of-function mutations in *PPD1* had a stronger effect on heading time than combined *co1 co2* mutations and, more importantly, *PPD1* was able to perceive and respond to differences in photoperiod in the absence of functional *CO1* and *CO2* genes. Similarly, *CO1* was able to accelerate heading time in response to LD in the absence of a functional *PPD1*. Taken together, these results indicate that *PPD1* and *CO1* are able to respond to photoperiod in the absence of each other, and that interactions between these two photoperiod pathways at the transcriptional and protein levels are important to fine-tune the flowering response in wheat.

**Author summary**

An understanding of the mechanisms involved in the regulation of wheat heading time is required to engineer more productive varieties better adapted to new or changing environments. A large proportion of wheat's natural variation in heading time is determined by differences in genes controlling the photoperiodic response. In this study, we show that the wheat *PHOTOPERIOD1* (*PPD1*) gene has a stronger effect on heading time than *CONSTANS1* (*CO1*) and *CO2* in the regulation of the photoperiodic response, and that complex genetic interactions among these genes are important to fine-tune heading time. Using loss-of-function mutants for both *CO1* and *CO2*, we demonstrate that these genes are not required for *PPD1* to perceive differences in photoperiod and regulate heading time. Similarly, we show that in the absence of *PPD1*, *CO1* can accelerate heading time more than 60 days in response to long days. Our results indicate that each of these two wheat photoperiod pathways can respond to differences in photoperiod even in the absence of the other one. Differences in the relative importance of these two pathways and in their epistatic interactions have contributed to the diversity of photoperiodic responses observed in different grass species.

## Introduction

A precise adjustment of flowering time to optimal environmental conditions is critical to maximize plant reproductive success. Plants have evolved complex regulatory mechanisms to adjust flowering initiation in response to seasonal changes and other environmental cues. Many plants, including the temperate cereals, require exposure to extended periods of cold (vernalization) to gain competence to flower [1]. After their vernalization requirement has been fulfilled, many plants still require inductive photoperiods to accelerate flowering. Based on their light requirements for floral induction, plants can be classified into long day (LD), short day (SD) or day-neutral plants [2].

The regulatory pathway that controls flowering in response to photoperiod is best characterized in the model plant *Arabidopsis thaliana*, a long day plant that flowers earlier when the days are longer than a critical threshold. In this species, the external coincidence model explains the integration of light signals with the circadian clock. The clock determines diurnal oscillations of the gene *CONSTANS* (*CO*), which results in the coincidence of the expression peak with the light phase under LD and with the dark phase under SD. Light stabilizes the CO protein, resulting in the induction of *FLOWERING LOCUS T* (*FT*) and the promotion of flowering under LD. Under SD, the degradation of the CO protein in the dark prevents the activation of *FT* [3-5]. Thus, *co* mutants in Arabidopsis flower later than wild type under LD but at the same time as wild type under SD [6].

CO belongs to a family of transcription factors characterized by two zinc finger B-Box domains at the N-terminus and by a CONSTANS, CONSTANS-like, TIMING OF CAB EXPRESSION 1 (CCT) domain at the C-terminus, a structure conserved in Arabidopsis and the grass homologs [7]. The *Oryza sativa* (rice) genome contains a single *CO* gene designated as *Hd1* [8], whereas

88 two paralogs designated as *CO1* and *CO2* have been identified in *Brachypodium distachyon*,
89 barley and wheat [9]. In the last three species, the predicted CO1 protein lacks conserved
90 cysteine residues at the start of the second B-box, suggesting a modified or non-functional B-box
91 2 in the temperate grasses [7, 9]. Phylogenetic and comparative genomics analyses suggest that
92 *CO1* and *CO2* paralogs originated by a segmental duplication at the base of the grass family,
93 with *CO1* located in the ancestral position colinear with rice *Hd1,* whereas *CO2* was lost in rice
94 and is likely not functional in sorghum [9]

95 Overexpression of *CO1* and *CO2* under the maize *UBIQUITIN* promoter in spring barley,
96 promoted flowering under both LD and SD conditions by upregulating *FT1* [10, 11]. However,
97 both *Ubi::CO1* and *Ubi::CO2* transgenic lines flowered 42-43 d later in SD than in LD
98 indicating the existence of additional genes controlling the photoperiodic response [10, 11]. In
99 barley, the response to photoperiod is determined mainly by the pseudo-response regulator gene
100 *PHOTOPERIOD1* (*PPD1*) [12], also known as *PRR37* in rice [13] and *Sorghum bicolor*
101 (sorghum) [14]. This gene is regulated by the circadian clock and the phytochrome-mediated
102 light signaling pathway and encodes a protein with a pseudo-receiver domain and a CCT domain
103 [14, 15].

104 In wheat, natural deletions in the promoter region of *PPD-A1* (*Ppd1-A1a*) and *PPD-D1* (*Ppd-*
105 *D1a*) are associated with increased transcript levels and accelerated heading under SD relative to
106 the ancestral *Ppd1b* allele [16, 17]. As a result, plants carrying the *Ppd1a* alleles show reduced
107 differences in heading time between LD and SD and are designated as photoperiod insensitive
108 (PI), whereas plants carrying the *Ppd1b* allele are designated as photoperiod sensitive (PS) [16,
109 17]. However, wheat PI lines still exhibit a significant acceleration of flowering under LD

110 relative to SD and, therefore, the wheat PI designation is used in this study to indicate a reduced
111 photoperiodic response rather than a lack of a photoperiodic response.

112 Under LD conditions, the wheat *PPD1* gene induces the expression of *FT1*, which encodes a
113 mobile protein that travels to the shoot apical meristem (SAM), where it promotes the expression
114 of the floral homeotic MADS box transcription factor *VERNALIZATION1* (*VRN1*) and the
115 synthesis of gibberellic acid (GA) [18]. The simultaneous presence of GA and *VRN1* results in
116 the up-regulation of *SUPPRESSOR OF OVEREXPRESSION OF CONSTANS1-1* (*SOC1*) and
117 *LEAFY* (*LFY*) genes, which are required for normal and timely spike development, stem
118 elongation and spike emergence or heading [18]. In photoperiod sensitive wheats grown under
119 SD, the SAM transitions to the reproductive stage, but stem elongation and spike development
120 proceed very slowly and heads fail to emerge or emerge extremely late [19]. These results
121 indicate that in wheat, the photoperiod pathway has a larger impact on the duration of spike
122 development and stem elongation than on the initial transition between the vegetative and
123 reproductive stages [18, 19]. The addition of gibberellic acid (GA) to PS spring wheat grown
124 under SD accelerates spike development, but only in lines that express *VRN1* under SD [18].

125 In addition to the natural PS and PI alleles, induced loss-of-function mutations in all *PPD1*
126 homeologs (henceforth, *ppd1*) have been developed for both hexaploid [20] and tetraploid wheat
127 [19]. These *ppd1* plants show large delays in heading time under LD and usually spikes emerge
128 very late, fail to emerge or are aborted under SD [19, 20]. The flowering phenotypes of the wheat
129 *ppd1* mutants are more drastic than those described for the barley photoperiod insensitive allele
130 *ppd-H1*, which has only amino acid changes and is likely a hypomorphic allele rather than a
131 complete loss-of-function allele [12]. It is important to differentiate the photoperiod insensitive

132 allele in barley that refers to delayed heading under LD, from the PI allele in wheat that refers to
133 accelerated flowering under SD.

134 *CO1* and *CO2* overexpression results in barley suggest a role of these genes as flowering
135 promoters [10, 11]. However, overexpression under a constitutive promoter results in elevated
136 transcript levels and ectopic expression in tissues or developmental phases that are different from
137 those of the natural alleles, which complicates the interpretation of overexpression results. The
138 use of loss-of-function mutations can provide a better understanding of the role of these genes
139 under more natural conditions. In this study, we investigate the role of *CO1* and *CO2* on the
140 photoperiod response in wheat using loss-of-function mutants for both genes in the tetraploid
141 spring wheat variety Kronos. In addition, we combine loss-of-function mutations in *co1*, *co2* and
142 *ppd1* to study the effect of their genetic interactions on heading time and on the transcription
143 profiles of critical flowering genes. We also investigate the interactions among the proteins
144 encoded by these genes. Taken together, these analyses show complex genetic interactions
145 among *CO1*, *CO2* and *PPD1* on heading time that reflect similarly complex interactions at the
146 transcriptional and protein levels.

147

148 **Results**

149 **Identification of *CO1* and *CO2* loss-of-function mutants in wheat**

150 We identified a total of 153 mutations in the A and B homeologs of *CO1* and *CO2* in the Kronos
151 tetraploid TILLING population [21, 22] using primers and PCR conditions listed in Supporting
152 Information Table S1. Among the 153 mutations, 74 resulted in non-synonymous amino acid
153 changes, and five introduced early stop codons resulting in truncated non-functional proteins

154 (Table S2). These five truncation mutations were validated by sequencing and one for each
155 homeolog was selected to study the function of *CO1* and *CO2* (Figure 1). We backcrossed the
156 individual mutant lines with wild-type Kronos at least twice to reduce background mutations.

157 We generated a *co1* loss-of-function mutant by crossing *co-A1* mutant T4-395 (Q242*) with *co-*
158 *B1* mutant T4-1170 (Exon2 acceptor splice site mutation). To generate the *co2* loss-of-function
159 mutant, we crossed *co-A2* mutant T4-202 (Exon 2 acceptor splice site mutation) with *co-B2*
160 mutant T4-391 (Q193*). Finally, we crossed the *co1* and *co2* mutants and generated a *co1 co2*
161 double mutant. The stop codon mutations in *co-A1* and *co-B2* truncate the carboxyl terminal half
162 of the CONSTANS protein including the CCT domain (Figure 1), which is critical for protein
163 function in both Arabidopsis and cereals [23]. Likewise, the splice-site mutations selected in the
164 *co-B1* and *co-A2* mutants result in intron retention and premature stop codons that also eliminate
165 the conserved CCT domain. Based on these large truncations we concluded that *co1 co2* has
166 loss-of-function mutations for all *CO1* and *CO2* homeologs.

167

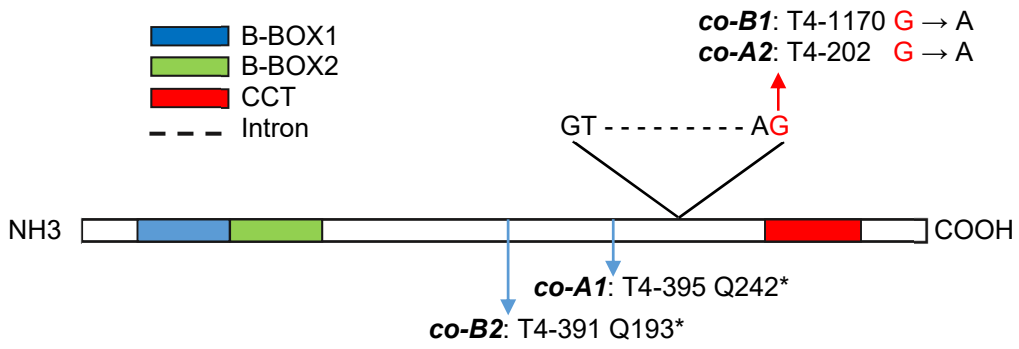


168
169

170 **Figure 1: *CO1* and *CO2* gene structure and position of the selected TILLING mutations.**
171 Both *CO1* and *CO2* genes have two exons, which encode two B-BOX domains at the N-terminus
172 and a CCT domain at the C-terminus. The selected *co-A1* and *co-B2* mutants have a premature

173 stop codon, whereas the *co-B1* and *co-A2* mutants have acceptor splice-site mutations that result
174 in intron retention and premature stop codons that eliminate the CCT domain. The T4 numbers
175 are the mutant identification. The schematic gene structure is based on *CO-A1* from Kronos
176 (GenBank MT043302).

177

178 **Effect of *PPD1* photoperiod sensitive (PS) and insensitive (PI) alleles on heading time and**
179 **spike development**

180 We transferred the four *co1 co2* mutations generated in Kronos-PI into a near-isogenic Kronos-
181 PS line [18] to study the effect of these mutations in two different backgrounds with large
182 differences in heading time under SD. To establish a baseline for comparison, we first describe
183 the effect of the two *PPD1* alleles in lines carrying the wild type *Co1* and *Co2* alleles (Figure
184 2A, blue bars).

185 Under LD, heading time was 2.5 d earlier in Kronos-PI (52.3 ± 0.4 d) than in Kronos-PS (54.8 ±
186 0.3 d). Although the difference was small, it was highly significant ($P < 0.0001$) and consistent
187 with previously published results [15]. Under SD, the differences between the two genotypes
188 were much larger (>66 d, $P < 0.0001$), with Kronos-PI heading at 113.2 ± 0.4 d and Kronos-PS
189 spikes failing to emerge before the experiment was terminated at 180 d. The earlier flowering of
190 Kronos-PI under SD reduced the difference between SD and LD in this genotype (61 d) relative
191 to Kronos-PS (>125 d, Figure 2A blue bars).

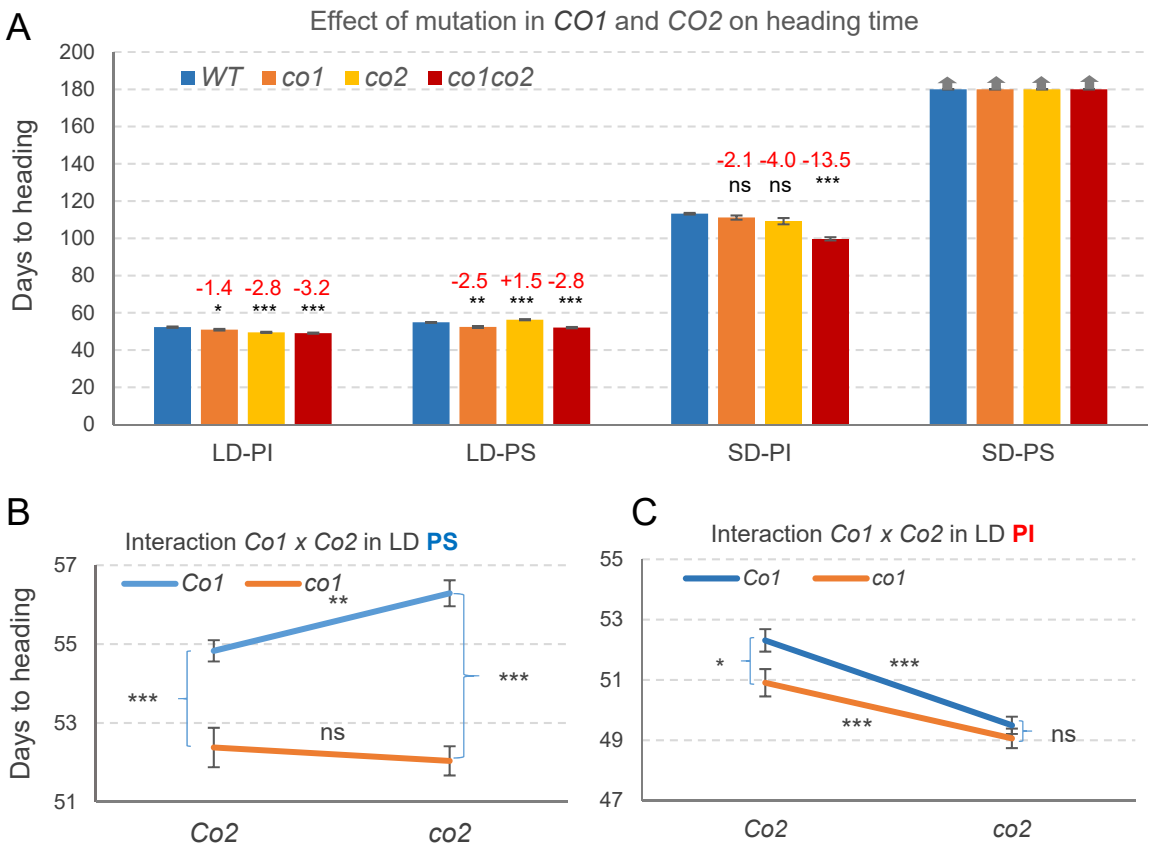


**Figure 2: Heading time of wild type, *co1, co2* and *co1 co2* mutants under LD and SD in Kronos-PI (*Ppd-A1a*) and Kronos-PS (*Ppd-A1b*) backgrounds**. (**A**) Averages are based on 15-19 plants in LD-PI (2 experiments), 21-24 plants in LD-PS (3 experiments) and 8 to 14 plants in SD-PI and SD-PS (1 experiment). Red numbers indicate differences in heading time relative to the wild type (mut-WT), with *P* values from a Dunnett test. Vertical arrows above the bars indicate that spikes have not emerged at 180 d (end of the experiment). (**B-C**) Interaction graphs for *CO1* and *CO2* in Kronos-PS (*Ppd-A1b*) and Kronos-PI (*Ppd-A1a*) backgrounds. The interactions was significant in B ($P = 0.0052$) but not in C (Table S3). Error bars are standard errors of the means (henceforth, s.e.m). *= $P < 0.05$, **= $P < 0.01$, ***= $P < 0.001$, ns= not significant.

204 To determine if the observed differences in heading time were the result of changes in the
205 duration of the vegetative phase or the spike development and elongation phases, we dissected
206 SAMs of the main tillers from the different genotypes (from 4- to 14-leaf stage, Figure S1).
207 Under LD, the SAMs from both Kronos-PI and Kronos-PS reached the early stages of spike
208 development by leaf four (W3-W3.25, Waddington scale [24]), the terminal spikelet stage
209 (W3.5) by leaf six, and headed at 52-55 d (Figure S1). Under SD, the SAMs of both genotypes
210 were at the vegetative stage by leaf four and started to elongate by leaf six. After that point, the
211 two genotypes diverged, while Kronos-PI transitioned to the terminal spikelet and lemma
212 elongation stage at the eighth leaf, Kronos-PS reached the same developmental stage at leaf 12
213 (Figure S1).

214

215 **Effect of *CO1* and *CO2* on heading time in the presence of functional *PPD1* alleles**

216 Loss of *CO1* and *CO2* function resulted in small but significant changes in heading time. The
217 *co1 co2* double mutant headed 3 d earlier than the wild type in both Kronos-PI and Kronos-PS ($P$
218 $< 0.0001$) under LD, and 13.5 d earlier than the wild type in Kronos-PI under SD ($P < 0.0001$,
219 Figure 2A). In the Kronos-PS background under SD, spikes failed to emerge or were aborted in
220 most of the plants by the end of the experiment at 180 d, limiting our ability to determine
221 difference on heading time between the *co1* and *co2* mutant and wild type alleles under this
222 condition.

223 Even though the differences in heading time between *co1 co2* and wild type alleles were larger
224 under SD (13.5 d) than under LD (3 d), they were still smaller than the differences between the
225 *PPD1* photoperiod sensitive and insensitive alleles under SD (>67 d), or the differences between
226 LD and SD in Kronos-PI (61 d) or Kronos-PS (>125, Figure 2A blue bars). These results

227 indicate that, in wheat, the *PPD1* alleles have a stronger effect on the photoperiodic response
228 than the *CO1* and *CO2* genes.

229 Except for the *co2* mutant that headed later than wild type in the Kronos-PS background under
230 LD (+1.5 d, $P < 0.0001$), all the other *co1* and *co2* single and double mutants headed
231 significantly earlier than their respective wild type controls under both LD and SD (Figure 2A).
232 These results suggest that under the tested conditions, *CO1* functions as a mild heading time
233 repressor in all backgrounds, and *CO2* as a mild heading time promoter or repressor depending
234 on the *PPD1* and *CO1* alleles present and the photoperiod (Figure 2A).

235 *Long day experiments*

236 To explore the interactions between *PPD1*, *CO1* and *CO2* under LD, we performed a factorial
237 ANOVA combining data from three experiments in Kronos-PS and two in Kronos-PI, using
238 experiments as blocks (nested within genotypes). This analysis showed highly significant effects
239 on heading time for *PPD1* ($P < 0.0001$), *CO1* ($P < 0.0001$) and *CO2* ($P = 0.0004$) and highly
240 significant two-way interactions for *PPD1* x *CO1* and *PPD1* x *CO2* ($P < 0.0001$, Table S3A).
241 The *CO1* x *CO2* interaction was not significant ($P = 0.3437$) but the three-way interaction was
242 significant ($P = 0.0046$, Table S3A), suggesting the possibility of different *CO1* x *CO2*
243 interactions in the different *PPD1* backgrounds that cancelled each other in the combined
244 analysis.

245 To test this possibility, we performed separate *CO1* x *CO2* factorial ANOVAs for Kronos-PS
246 and Kronos-PI. In the Kronos-PS background, *CO1* showed a stronger effect ($P < 0.0001$) on
247 heading time than *CO2* ($P = 0.1448$) and their interaction was significant ($P =0.0052$, Figure 2B,
248 Table S3B). By contrast, in the Kronos-PI background, *CO2* showed a stronger effect ($P <$
249 $0.0001$) than *CO1* ($P = 0.0157$) and the interaction was not significant. ($P = 0.1934$, Figure 2C,

250 Table S3C). In summary, these results indicate complex genetic interactions between *PPD1*,
251 *CO1* and *CO2* in the regulation of heading time under LD.

252 *Short day experiments*

253 Under SD, the Kronos-PS lines failed to flower before the experiment was terminated (180 d), so
254 we were only able to study the interactions between *CO1* and *CO2* in the Kronos-PI background.
255 All four genotypes headed between 100 and 113 d, which is 51 to 61 d later than the same lines
256 under LD. A factorial ANOVA for heading time showed significant effects for both *CO1* and
257 *CO2* ($P < 0.0001$) and a significant interaction between the two ($P = 0.0029$, Table S4). This
258 interaction was associated with the larger acceleration of heading time in the double mutant (13.5
259 d) than in the single *co1* (2.1 d) and *co2* (4.0 d) mutants (Figure 2A). This result indicates a
260 stronger effect of each mutation in the presence of the mutant allele of the other gene than in the
261 presence of the wild type allele (Table S4).

262 To see if the *co1* and *co2* mutations in the Kronos-PS background were associated with delays in
263 SAM differentiation or in spike development, we dissected apices for three plants from each
264 genotype every week from 4 to 11 weeks, and included wild type Kronos-PI as a control. Under
265 SD, all five genotypes reached the double-ridge stage (W2.5) by week 6 (Figure 3A-B). From
266 there, the Kronos-PI genotype developed more rapidly than the four Kronos-PS genotypes,
267 which showed similar developmental rates in the wild type and the *co1* and *co2* mutants (Figure
268 3B). By week 11, the developing spikes in the Kronos-PI control were 3-13 cm long including
269 awns, the peduncles were 5 to 14 mm long, and the developing flowers were at the elongated
270 stigmatic branches stage (>W7.5). By contrast, all four Kronos-PS lines at the same time point
271 showed no peduncle elongation, produced spikes of less than 0.5 cm, and the flowers still had the
272 stylar canal open (<W6.0). These results indicate that the *co1* and *co2* mutations have a limited

273 effect on spike development and elongation in the Kronos-PS background under SD compared

274 with the strong effect of the *Ppd-A1a* in Kronos-PI.

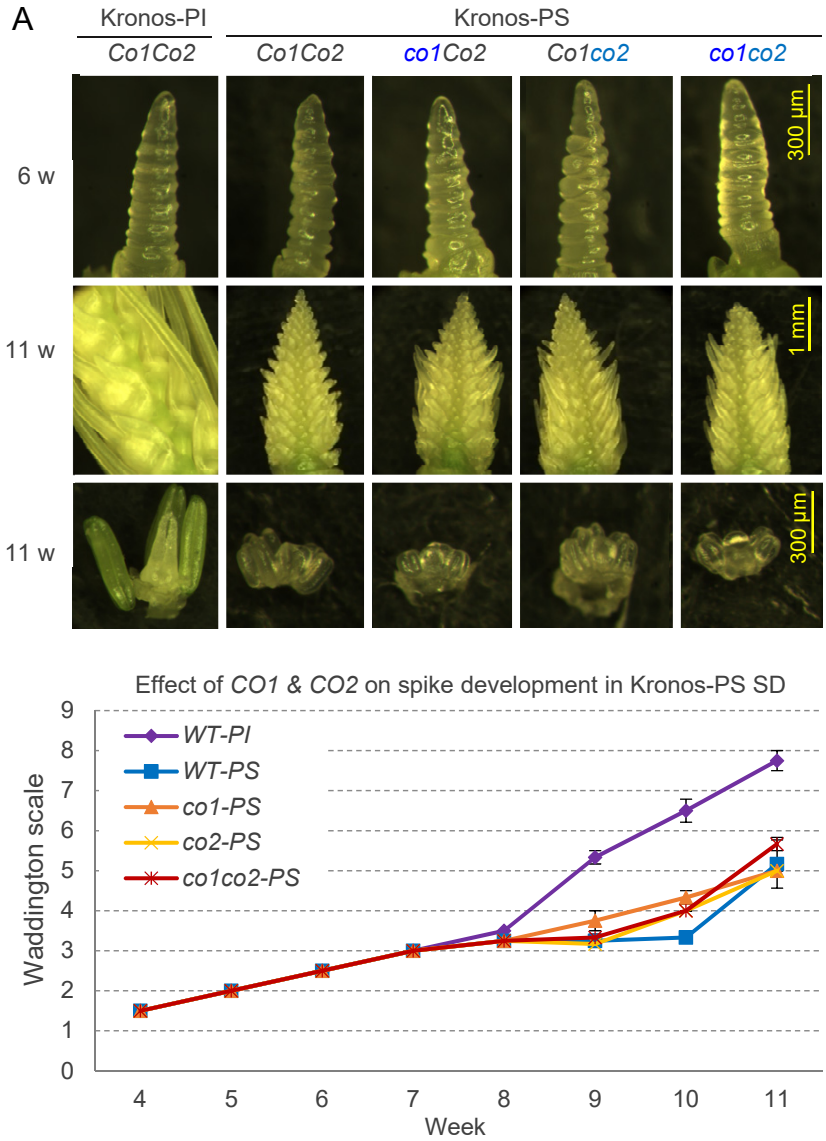


275

276 **Figure 3. Effect of *co1* and *co2* mutations on spike development in Kronos-PS under SD.**

277 Kronos-PI was included as control. (**A**) Dissecting microscope images of developing apices at

278 week 6 (double-ridge, W2.5) and week 11 with a detail of their floral organs. (**B**) Developmental

279 time course of SAM using the Waddington scale from 4- through 11-week-old plants (n = 3).
280 Error bars are standard errors of the means.

281

282 **Effect of *CO1* and *CO2* on heading time in the absence of functional *PPD1* alleles**

283 To investigate the effect of *CO1* and *CO2* in the absence of *PPD1*, we introgressed the *co1* and
284 *co2* mutations into a Kronos line with loss-of-function mutations in both *PPD-A1* and *PPD-B1*
285 (*ppd1*) [19]. As before, we describe first the differences in SAM development and heading time
286 between Kronos-PS and *ppd1* mutants carrying the wild type *Co1* and *Co2* alleles to establish a
287 baseline for comparison (Figure 4A, blue bars).

288 Under LD, the plants with the *ppd1 Co1 Co2* allele combination headed much later (115.5 ± 15.3
289 d) than the Kronos-PS controls carrying the functional *Ppd1b* allele (52.5 ± 0.7 d, Figure 4A),
290 similar to results reported before [19]. The *ppd1* mutant plants showed a 79% reduction in
291 number of grains per spike relative to the Kronos-PS lines (Figure 4B-C). Apex dissections
292 showed a delayed transition to the double-ridge stage in the *ppd1* mutant (leaf 8 to 10) relative to
293 Kronos-PS (<leaf 4, Figure S1). Similarly, the terminal spikelet was formed in Kronos-PS by
294 leaf 6 but was not formed in *ppd1* by leaf 14, when the experiment was terminated (Figure S1).
295 Under SD, spikes of both the *ppd1* mutant and Kronos-PS failed to emerge by 180 d. Dissection
296 of the main tillers from these plants showed that spike development in *ppd1* lagged behind that
297 of Kronos-PS (Figure S1, leaf 12 and 14 and Figure S2). These results indicate that *PPD1* is not
298 essential for the initial transition of the SAM to the reproductive stage, but in its absence, spike
299 development and stem elongation are severely compromised.

300

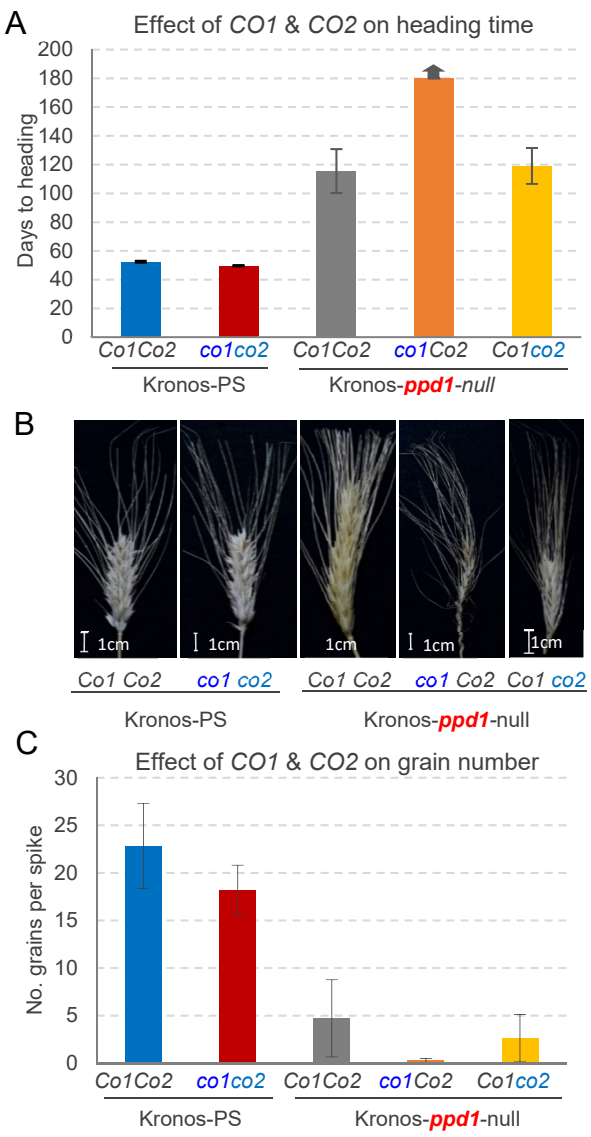


**Figure 4. Phenotypic effects of *co1* and *co2* mutations in the absence of functional *PPD1* genes under LD** (**A**) Average days to heading in *ppd1* mutants carrying mutations in either *co1* or *co2*. Kronos-PS wild type and *co1 co2* double mutants are included as controls. The arrow on top of the bar indicates that most plants failed to flower before the experiment was terminated at 180 d. (**B**) Spike phenotypes at the end of the experiment (180 d). (**C**) Number of grains per spike recovered from the same genotypes as in A. Error bars are standard errors of the means calculated from 7 to 16 plants per genotype for flowering and from 4 to 8 plants for grain number.

322 The introgression of the *co2* mutation in the *ppd1* background had a limited effect on heading
323 time. Heading time of the double mutant *ppd1 co2* (119.1 ± 12.5 d) was only four days later than
324 *ppd1*, and the differences were not significant suggesting a limited effect of *CO2* on heading
325 time in the absence of a functional *PPD1*. The *ppd1 co2* double mutant showed an even more
326 severe reduction in grain production than the *ppd1* mutant (89% reduction relative to Kronos-
327 PS), but the differences were not significant.

328 The most important result was observed when we combined the *ppd1* and *co1* mutations. The
329 spikes from the *ppd1 co1* plants failed to emerge before the experiment was terminated at 180 d
330 (Figure 4A), and failed to produce any grains (Figure 4B-C). Even though we were not able to
331 recover the triple *ppd1 co1 co2* mutant, the delayed heading time of the *ppd1 co1* mutant relative
332 to the *ppd1* and *ppd1 co2* mutants (>60d) is sufficient to conclude that *CO1* can accelerate
333 heading time in response to LD even in the absence of functional *PPD1* alleles.

334

335 **Effect of mutations in *PPD1*, *CO1* and *CO2* on the transcriptional profiles of flowering**
336 **genes**

337 To better understand the regulatory networks underlying the genetic interactions described
338 above, we characterized the effect of loss-of-function mutations in *PPD1, CO1* and *CO2* in a
339 Kronos-PS background on the transcription profiles of several flowering genes. We grew the
340 plants in a growth chamber under LD and sampled the fully expanded fourth leaf every 4 hours
341 throughout a 24-h period.

342 *CO1* transcripts were significantly upregulated in both *co2* and *ppd1* mutants 12 hours after the
343 start of the light phase (Zeitgeber time 12 or ZT12, Figure 5A), suggesting that these two genes

act as transcriptional repressors of *CO1*. The negative effect of *PPD1* on *CO1* transcription was also observed in a separate experiment using older plants (six-week-old). In leaf samples collected at ZT4 we observed a significant upregulation of *CO1* in the *ppd1* and *ppd1 co2* mutants relative to Kronos-PS (Figure S3A). No differences were detected between the *ppd1* and *ppd1 co2* mutants, which suggests that the loss of *co2* function did not affect *CO1* expression in the absence of functional *PPD1* genes (Figure S3A). Transcript levels of *CO2* were very low and showed no significant differences among genotypes (Figure 5B). We further confirmed these observations in six-week old plants of Kronos-PS, *ppd1* and *ppd1 co1* plants sampled at ZT4 (Figure S3B).

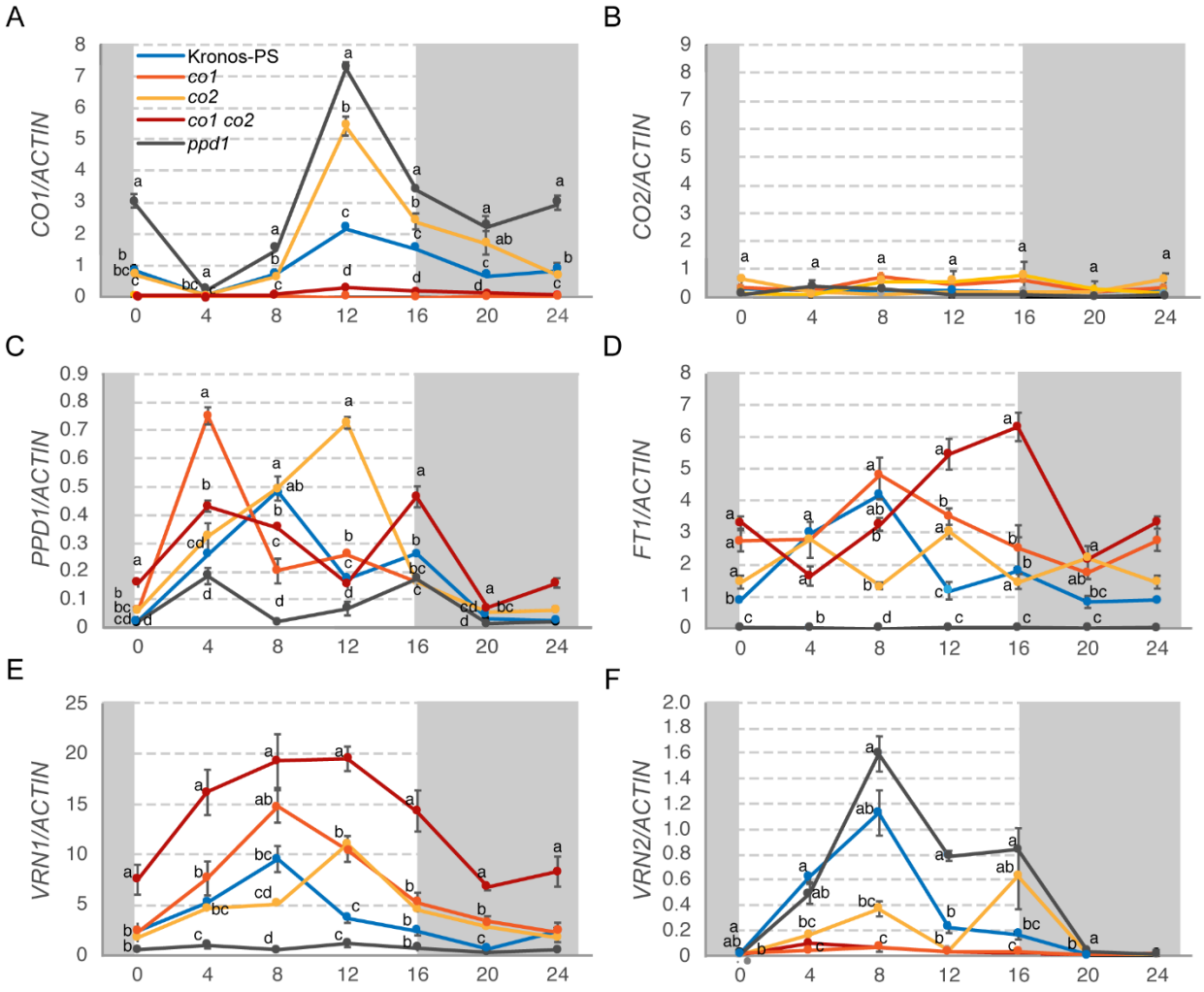

354

355 **Figure 5.** Effect of loss-of-function mutations in *CO1*, *CO2* and *PPD1* in Kronos-PS on the
356 transcriptional profiles of wheat flowering genes under LD. (**A**) *CO1*, (**B**) *CO2*, (**C**) *PPD1*, (**D**)
357 *FT1*, (**E**) *VRN1*, (**F**) *VRN2* in Kronos-PS, *co1*, *co2*, *co1 co2* and *ppd1* mutants. We grew the
358 plants in a growth chamber under 16 h light at 22 °C and 8 h darkness at 17 °C (gray areas).
359 Fully expanded 4$^{th}$ leaves (Zadoks scale =14) were harvested at ZT0, ZT4, ZT8, ZT12, ZR16,
360 and ZT20. The ZT0 value is the same as at ZT24. Shaded boxes represent night. Values are
361 averages of four biological replicates and bars are SE of the means. Expression values are
362 relative to *ACTIN* using the delta Ct method. Primers and primer efficiencies are listed in Table
363 S5 (all amplify both A and B homologs of the respective genes).

364

365 The *PPD1* gene in Kronos-PS showed a main peak in the middle of the light period (ZT8) and a
366 secondary peak at dusk (ZT16), which is consistent with the *PPD1* profile previously described
367 in the photoperiod sensitive *T. monococcum* [25]. In the *co1* and *co1 co2* mutants, the main peak
368 was shifted 4 h earlier (ZT4), whereas in the *co2* mutants the main peak was delayed 4 h (ZT12,
369 Figure 5C). The ZT16 peak was significantly higher than the wild type in the *co1 co2* double
370 mutant but not in the single mutants (Figure 5C). The complex effects of the *co1* and *co2*
371 mutations on *PPD1* transcription profiles reflect the significant two- and three-way genetic
372 interactions among these three genes on heading time described above.

373 The *FT1* profile was similar to that of *PPD1* in wild type Kronos-PS, but not in the *co1* and *co2*
374 mutants (Figure 5D). The two profiles were also similar in the upregulation of the secondary
375 peak at ZT16 in the *co1 co2* double mutant, which correlates with the earlier heading time of this
376 mutant under LD. The earlier heading time of *co1 co2* also correlated well with the significantly

377 higher transcript levels of *VRN1* in this mutant (Figure 5E). We observed a significant reduction
378 of the transcript levels of *FT1* and *VRN1* in the *ppd1* mutant relative to wild type, which is
379 consistent with its delayed heading time.

380 The *VRN2* locus includes two genes, but since *ZCCT1* is not functional in tetraploid wheat [26],
381 we present only expression data for *ZCCT2*. The transcriptional profiles of *PPD1* and *ZCCT2*
382 were similar for the wild type Kronos-PS but not for the different mutants (Figure 5). We
383 observed a small but not significant increase of *ZCCT2* transcript levels in the *ppd1* mutant and a
384 significant downregulation in the *co1* and *co1 co2* mutants. The interpretation of these results is
385 complicated by the effects of these mutants on *VRN1* which is a known repressor of *VRN2* [27]
386 (see Discussion section).

387

388 **Effect of *VRN1* on the transcriptional regulation of *CO1* and *CO2***

389 To explore the potential role of *VRN1* in the transcriptional regulation of *CO1* and *CO2*, we used
390 Kronos *vrn-A1* and *vrn-B1* single mutants and *vrn-A1 vrn-B1* double mutant (henceforth *vrn1*)
391 developed previously [27]. The *vrn-B1* mutant has a functional allele of *VRN-A1* that confers a
392 dominant spring growth habit, whereas the *vrn-A1* mutant has the ancestral allele of *VRN-B1* that
393 confers a recessive winter growth habit. The *vrn1* double mutant has a delayed heading time and
394 a residual response to vernalization [27].

395 *CO1* showed significantly higher transcript levels in the late flowering *vrn-A1* and *vrn1* mutants
396 than in the rapidly flowering *vrn-B1* mutant, both in vernalized and un-vernalized plants (Figure
397 6 A-B). In all genotypes, *CO1* was downregulated to very low levels in the flag-leaf at heading
398 time. In the *vrn1* mutant, we observed a slight decrease of *CO1* transcript levels during

399 vernalization followed by a rapid upregulation when we moved the plants back to room
400 temperature (RT). By contrast, in the single *vrn-A1* and *vrn-B1* mutants, which still have one
401 functional copy of *VRN1*, *CO1* transcripts stayed low after the plants were returned to RT
402 (Figure 6 A). From previous studies, we know that *VRN1* transcript levels increase slowly during
403 LD vernalization and then rapidly when plants are moved to RT and start to flower [27]. Taken
404 together, these results suggest that *VRN1* acts as a transcriptional repressor of *CO1*.

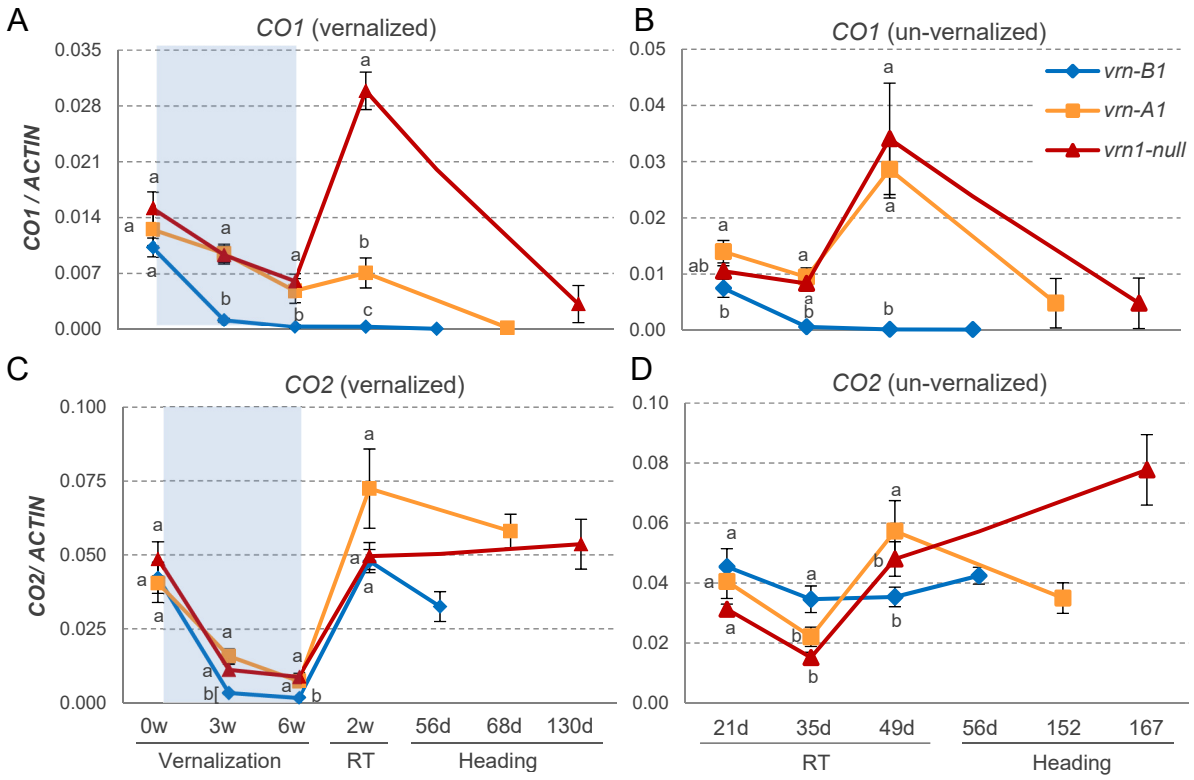


405

406 **Figure 6.** Effect of mutations in Kronos *vrn-A1* (winter growth habit), *vrn-B1* (spring growth
407 habit) and *vrn-A1 vrn-B1* (*vrn1* very late heading) on the transcriptional profiles of *CO1* and
408 *CO2*. All mutants are homozygous and in the Kronos-PI background. (**A-B**) *CO1* and (**C-D**)
409 *CO2* transcription profiles. **A** & **C**) More recently expanded leaves from three weeks old plants
410 were sampled before vernalization (0w), at 3w and 6 w vernalization (4°C), 2 weeks after return
411 to room temperature (RT= 22°C day and 18°C) and at heading time (HT), which was different

412 for each genotype. **B** & **D**) Same genotypes but grown at RT without vernalization. Points are
413 averages of eight plants and error bars are standard errors of the means. Means with different
414 letters are significantly different in Tukey test for that time point ($P < 0.05$). Note that the
415 upregulation of *CO1* after the return of the plants from vernalization occurred only in the *vrn1*
416 mutant that has no functional copies of *VRN1*.
417

418 *CO2* transcripts were downregulated during vernalization and showed a sharp increase when we
419 moved the plants to RT. However, in contrast to *CO1*, this increase was observed in all three
420 genotypes (Figure 6C-D). After this increase, *CO2* transcript levels remained high in the flag
421 leaves during heading and showed no significant differences between the *vrn1* and the spring
422 *vrn-B1* mutant (Figure 6C-D). These results indicate that *VRN1* has a smaller effect on the
423 regulation of *CO2* than on the regulation of *CO1*.
424

425 **Effect of photoperiod and phytochromes on the transcriptional regulation of *CO1* and *CO2***

426 The strong upregulation of *CO1* in the *ppd1* mutant indicated that *PPD1* is a transcriptional
427 repressor of *CO1* (Figure 4A). Since phytochromes *PHYC* [15] and *PHYB* [28] are both required
428 for the LD transcriptional activation of *PPD1*, we explored the effect of mutations in these two
429 phytochromes on the expression profiles of *CO1* and *CO2*. To do this, we used recently
430 published RNAseq studies for leaf samples ($4^{th}$ leaf, ZT 4h) from loss-of-function mutants *phyB*
431 and *phyC* in Kronos-PI under both LD [28] and SD conditions [29].

432 A factorial ANOVA for transcripts per million reads (TPM) using photoperiod (LD and SD) and
433 genotype (WT, *phyC* and *phyB*) as factors, revealed significant differences between SD and LD

434 for all four genes (*CO-A1*, *CO-B1*, *CO-A2* and *CO-B2*, Figure S4). We also detected difference
435 between genotypes and genotype x photoperiod interactions for the *CO1* homeologs but not for
436 the *CO2* homeologs. The significant interaction was associated with the LD downregulation of
437 *CO1* homeologs in the wild type and their upregulation in the *phyB* and *phyC* mutants (Figure
438 S4). Both *CO2* homeologs were upregulated by LD and showed no significant differences
439 between wild type and *phy* mutants. *CO-B2* showed significantly higher transcript levels than
440 *CO-A2* for all genotypes (Figure S4), whereas for *CO1* the transcript levels and the differences
441 were larger in *CO-A1* relative to *CO-B1*.

442

443 **Protein-protein interactions among CO1, CO2, PPD1, VRN2, PHYC and PHYB**

444 To test if the interactions among *CO1*, *CO2* and *PPD1* observed at the genetic and
445 transcriptional levels were associated with interactions at the protein level, we performed yeast-
446 two-hybrid (Y2H) and split yellow fluorescent protein (YFP) assays among the three proteins. In
447 a previous study, we reported positive Y2H interactions between the CCT domains of CO1 and
448 CO2, but not between these two proteins and a truncated version of PPD1 including the CCT
449 domain [30]. In this study, we used a complete PPD1 protein and detected strong Y2H
450 interactions between PPD1 and both CO1 and CO2. The Y2H interaction between PPD1 and
451 CO1 was stronger than between PPD1 and CO2 (Figure 7A).

452 We further validated the interactions between CO1 and CO2 (Figure 7B) and between CO1 and
453 PPD1 (Figure 7C-D) using split-YFP assays in wheat protoplasts. We initially failed to detect the
454 split-YFP interaction between CO1 and PPD1 in Kronos, so we used protoplasts extracted from
455 an early flowering loss-of-function mutant for *elf3* in Kronos, which has increased levels of
456 *PPD1* transcripts [25, 31]. We were able to detect the CO1-CO2 and CO1-PPD1 interactions

457 (but not the CO2-PPD1) by split-YFP in the *elf3* mutant when protoplasts were exposed to light.
458 For both CO1 and PPD1, we detected the proteins by Western blots only after we exposed the
459 protoplasts to light but not when we incubated them in the dark after transfection, suggesting that
460 light is required to stabilize these proteins.

461
462
463
464
465
466
467
468
469
470
471
472
473

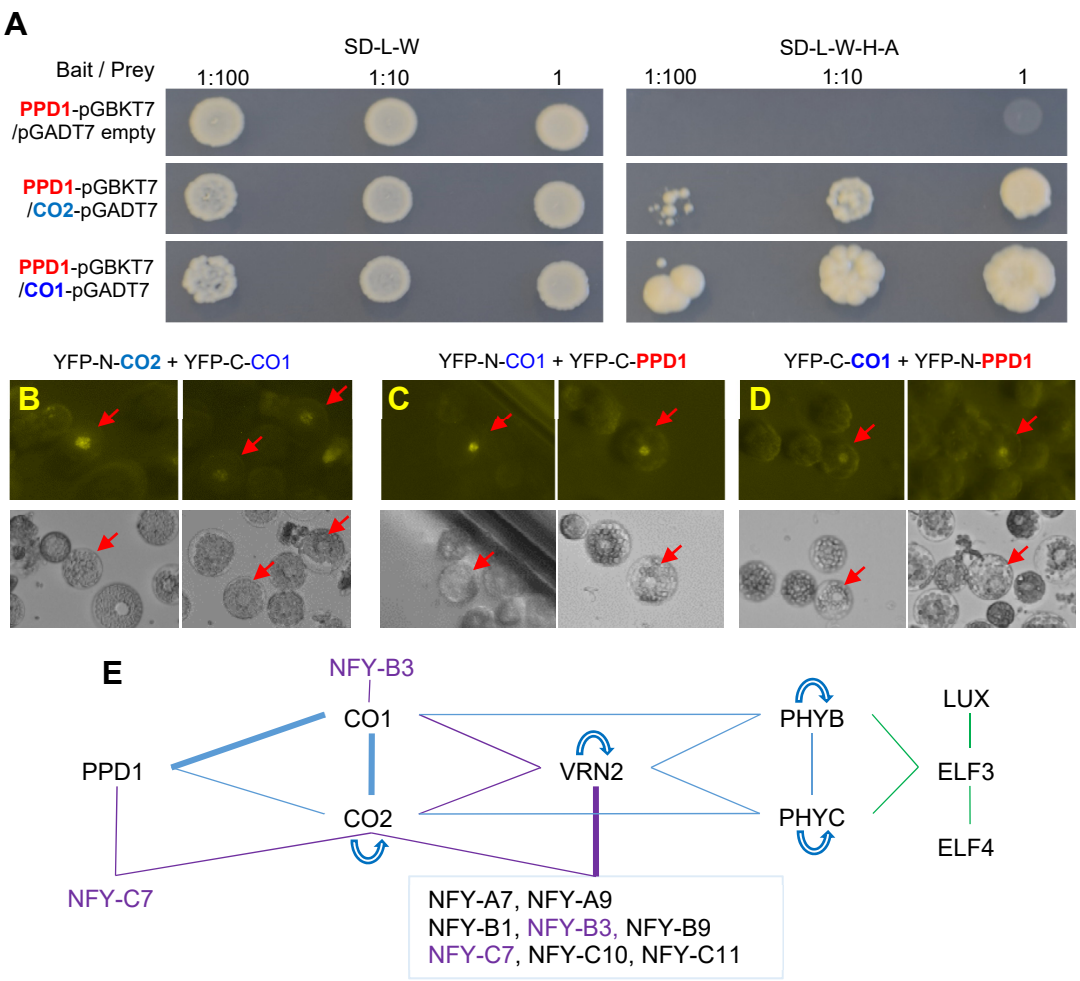


474

475 **Figure 7. Protein interactions**. (**A**) Yeast-two-hybrid (Y2H) interactions between PPD1 and
476 CO1 or CO2. Left panel: SD medium lacking Leucine and Tryptophan (SD-L-W) to select for
477 yeast transformants containing both bait and prey. Right panel: interaction on SD-L-W-H-A
478 medium (no L, W, H and A). Dilution factors = 1, 1:10 and 1:100. (**B-D**) Split-YFP in wheat

479 protoplast. (**B**) Positive nuclear interactions between CO1 and CO2. (**C-D**) Positive nuclear
480 interactions between CO1 and PPD1 in two different YFP-N/YFP-C configurations. (**E**)
481 Summary of Y2H interactions among wheat CO1, CO2, PPD1, VRN2, PHYB, PHYC, and ELF3
482 from Figure S5. Green lines are based on published results from *Brachypodium* [32] and violet
483 lines on published results from wheat [24]. Thick lines indicate interactions validated by split-
484 YFP in wheat protoplasts (blue) or *in vitro* coIP (violet). Curved arrows indicate self-
485 dimerization**.**

486

487 Finally, we tested pairwise interactions among CO1, CO2, PPD1, VRN2, PHYC and PHYB
488 proteins by Y2H assays (Figures 7E and S5). In addition to interacting with CCT-domain
489 proteins PPD1 (Figure 7A) and VRN2 [30], CO1 and CO2 showed positive interactions with
490 both PHYC and PHYB (Figure 7E and S5) in the Y2H assays. The interaction between CO1 and
491 PHYC was stronger than between CO1 and PHYB, whereas the interaction between CO2 and
492 PHYB was stronger than between CO2 and PHYC. Both phytochromes showed positive
493 interactions with VRN2 but not with PPD1 (Figures 7E and S5). In addition, we showed that the
494 full length PPD1 protein did not interact with VRN2 in Y2H (Figure S5). CO2, VRN2, PHYC
495 and PHYB were able to form homodimers [15, 30] but not CO1 or PPD1 (Figure S5). The
496 diagrammatic representation of these interactions reveals an extensive and complex network of
497 protein-protein interactions, with CO1 and CO2 providing a connection between the LD
498 flowering promoter PPD1 and the LD flowering repressor VRN2 (Figure 7E).

499

500

501

502 **Discussion**

503 **Genetic interactions among *CO1*, *CO2, PPD1* and *VRN2* modulate photoperiodic responses**
504 **in grasses**

505 ***Long day grasses***

506 Natural variation in wheat heading time in response to photoperiod has been mapped mainly to
507 the three *PPD1* homeologs [16, 17, 33]. Similarly, a genome wide association study of 220
508 spring barley varieties found that most of the variation in heading time (31%) was associated
509 with the *PPD1* locus and variation in the *CO1* locus had a limited contribution (<5%) [34].
510 These results agree with the limited effect on heading time detected in this study in the Kronos
511 *co1*, *co2*, and *co1 co2* mutants compared with the large differences detected between *PPD1*
512 alleles (Figure 2) and mutants (Figure 4). Even when both *CO1* and *CO2* homeologs were
513 replaced with truncated mutants (*co1 co2*), plants headed only three days earlier than the wild
514 type under LD and 13 days earlier under SD (Figure 2). By contrast, loss of function mutations
515 in *PPD1* delayed heading time approximately two months in LD (Figure 4), and differences
516 between the *Ppd-A1a* and *Ppd-A1b* alleles were even larger under SD (Figure 2).

517 The effect of the *co1 co2* mutations on the acceleration of heading time was small, but highly
518 significant ($P < 0.0001$) and consistent across experiments under both LD and SD (Figure 2).
519 This was an unexpected result because transgenic barley plants overexpressing *CO1* [10] or *CO2*
520 [11] flowered earlier than the wild type under both LD and SD. These transgenic results had led
521 to the general assumption that *CO1* and *CO2* operate as flowering promoters in the temperate
522 grasses. However, our results show that when *CO1* and *CO2* are expressed under their native
523 promoters in their expected tissues and developmental stages (and in the presence of functional

524 *PPD1* and *VRN2* alleles) they operate mainly as mild LD and SD flowering repressors rather
525 than as flowering promoters (except for *CO2* in Kronos-PS under LD, Figure 2).

526 This inconsistency may be generated by the elevated and ectopic expression levels of *Ubi::CO1*
527 and *Ubi::CO2* in the transgenic plants, but also by differences in the genetic backgrounds. The
528 two transgenic barley lines were developed in the variety Golden Promise [10], which carries the
529 *ppd-H1* allele with reduced sensitivity to LD and does not have any functional copy of *VRN2*. By
530 contrast, Kronos has functional *PPD1* and *VRN2* genes. Our results show that in a Kronos line
531 with no functional copies of *PPD1* (*ppd1*), *CO1* accelerates heading time under LD (Figure 4)
532 similarly to the overexpression of *CO1* in Golden Promise. In addition, the downregulation of
533 *VRN2* in the Kronos *co1 co2* mutant may have contributed to the earlier heading time of these
534 mutants (Figure 2), whereas no interactions with *VRN2* are possible in Golden Promise.

535 The previous results suggest the existence of complex genetic interactions among the
536 photoperiodic genes, a hypothesis that is also supported by significant digenic interactions in the
537 factorial ANOVA including *CO1*, *CO2* and *PPD1* (Table S3). The three-way interaction among
538 the three genes was also significant, which reflects the significant interaction between *CO1* and
539 *CO2* in Kronos-PS but not in Kronos-PI (Table S3). The contribution of the *PPD1* x *CO2*
540 interaction to the total sum of squares (9%) was more than two-fold higher than the main *CO2*
541 effect (4%), which suggests that a large part of *CO2* effect on heading time was mediated by its
542 modulation of the *PPD1* function (Table S3). Strong genetic interactions between *CO1* and
543 *PPD1* on heading time have also been reported in a barley biparental population segregating for
544 *Ubi::CO1* and the *ppd-H1* mutation [10] and in two genome wide association studies (GWAS) in
545 spring barley [34, 35]. In both GWAS, significant effects of *CO1* on heading time were detected
546 among the lines carrying the *ppd-H1* allele but not among the lines carrying the wild type *Ppd-*

547 *H1* allele [34, 35]. These strong genetic interactions indicate that the effect of a particular
548 photoperiod gene depends strongly on genetic background, a result that has been also reported in
549 the SD grasses as described below.

550 ***Short day grasses***

551 In most sorghum genotypes, *SbCO1* operates as a flowering promoter in SD and as a flowering
552 repressor in LD [36] and *SbPRR37* as a flowering repressor in LD [14, 37]. By contrast, the
553 orthologous *PPD1* gene in barley and wheat functions as a LD heading promoter [12, 16, 19]
554 (Figure 4). In spite of the opposite roles, the genetic interactions between *PRR37/PPD1* and *CO1*
555 showed some similarities. In a sorghum population segregating for *SbCO1* and *SbPRR37*, *SbCO1*
556 showed a large effect on heading time among the plants carrying the non-functional *Sbprr37*
557 allele (48% of the variation), but had no effect among the plants carrying the functional *SbPrr37*
558 allele [38]. This is similar to the GWAS results in spring barley described above [34, 35] and to
559 the stronger effect of the *co1* mutation in the *ppd1* mutant than in the Kronos plants with
560 functional *PPD1* alleles described in this study.

561 Similar to sorghum, in most rice genotypes, *OsPRR37* (=*Hd2*) works as a LD flowering
562 repressor [13] and *OsCO1* (=*Hd1*) as both a LD flowering repressor and a SD flowering
563 promoter. Interestingly, transformation of a rice line deficient in *OsCO1* function with a wheat
564 *CO2* genomic clone accelerated flowering in SD and delayed flowering in LD, complementing
565 the *OsCO1* function [39]. Since our results indicate that wheat *CO2* functions as a SD flowering
566 repressor (Figure 2A), the rice result suggests that the function of the wheat CO2 protein was
567 altered when it was expressed in rice. The opposite change was observed when a late-flowering
568 Arabidopsis *prr7* mutant was transformed with rice *OsPRR37* driven by the Arabidopsis *PRR7*
569 promoter. When expressed in Arabidopsis, *OsPRR37* functioned as a LD promoter of flowering

570 in spite of its normal role as a LD repressor of flowering in rice. Based on these results, it is
571 tempting to speculate that the different roles of *PRR37/PPD1* and *CO2* in SD and LD grasses
572 may be the result of differences in the balance of multiple epistatic interactions among the genes
573 involved in the photoperiodic response, rather than a difference in the specific function of their
574 encoded proteins.

575 This hypothesis is also supported by changes in gene function reported in sorghum and rice
576 plants carrying loss-of-function mutations in both *PRR37* (*prr37*) and *GRAIN NUMBER, PLANT*
577 *HEIGHT, AND HEADING DATE7* (*ghd7,* a *VRN2* ortholog [40]). In the *prr37 ghd7* sorghum
578 and rice mutants, *CO1* function changed from a flowering repressor to a flowering promoter in
579 LD, while maintaining its usual role as a flowering promoter in SD [38, 41, 42]. In addition, in
580 most rice genotypes carrying the *ghd7* mutation *OsPRR37* function changes from a SD promoter
581 to a SD repressor of heading, while maintaining its role as a LD flowering repressor [43].
582 Genetic interactions between *VRN2* (*GHD7*) and both *CO1* (*Hd1*) [44] and *CO2* [11] have been
583 reported also in barley, suggesting that similar mechanisms may exist in the temperate cereals.
584 Taken together, these results indicate that genetic interactions between *PPD1/PRR37*,
585 *VRN2/GHD7* and *CO1/CO2* play a central role in the regulation of heading time in response to
586 photoperiod in both LD- and SD-grasses and that, therefore, the effect of particular genes may
587 vary in different genetic backgrounds.

588

589 **Complex interactions at the transcriptional level contribute to the observed genetic**
590 **interactions on heading time**

591 The significant upregulation of *CO1* in the *ppd1* mutant (Figure 5A and Figure S3A) suggests
592 that *PPD1* may function as a transcriptional repressor of *CO1*. This hypothesis is supported by

593 the upregulation of *CO1* in the *phyB* and *phyC* mutants (Figure S4), where *PPD1* transcription is
594 strongly downregulated [15, 28], and by the negative correlation between *PPD1* and *CO1*
595 transcript levels in both *ppd1* triple mutants of hexaploid wheat 'Paragon' under LD [20], and
596 photoperiod sensitive and insensitive isogenic lines of Paragon under SD [45].

597 However, since *PPD1* induces the expression of *VRN1*, which represses *CO1* transcription
598 (Figure 6), we cannot rule out the possibility that the effect of *PPD1* on *CO1* transcription is
599 mediated by *VRN1*. When Kronos *vrn-A1*, *vrn-B1* and *vrn1* mutants were returned to room
600 temperature after vernalization, *CO1* was rapidly upregulated in the leaves of the *vrn1* mutant
601 but not in the other three genotypes with functional *VRN1* copies (Figure 6). An identical
602 expression profile has been described before for *VRN2* in the same mutants [27], indicating that
603 *VRN1* functions as a transcriptional repressor of both *CO1* and *VRN2*.

604 *CO2* transcript levels were not significantly affected by *PPD1*, *CO1* (Figure 5B) or *VRN1*
605 (Figure 6C-D). Similarly, no changes in *CO2* transcription were observed between Paragon-PI
606 and Paragon-PS lines grown under SD [45], between Kronos-PI and the *phyB* or *phyC* mutants
607 (Figure S4), or between Kronos-PS and *ppd1* mutants (Figure S3B). However, mutations in *co2*
608 affected the diurnal transcriptional profiles of all the flowering genes presented in Figure 5. *CO1*
609 transcript levels were more than 2-fold higher in the *co2* mutant than in the Kronos-PS control at
610 the ZT12 peak (Figure 5A), suggesting that CO2 functions as a negative transcriptional regulator
611 of *CO1*. This is also supported by the downregulation of *CO1* transcripts in a barley line
612 overexpressing *CO2* [11]. The effect of *CO2* on *CO1* transcription may contribute to the
613 significant genetic interaction on heading time observed between *CO1* and *CO2* in this study
614 (Table S3b).

615 Overexpression of *CO1* and *CO2* in winter barley was associated with the upregulation of *VRN2*,
616 both under LD and SD, where *VRN2* is not normally expressed [11]. A similar upregulation of
617 *VRN2* has been reported in *Brachypodium* plants overexpressing *CO1* under LD [46]. By
618 contrast, knock-down of *CO1* expression in *Brachypodium* [46] or loss-of-function mutants in
619 *co1*, *co2*, or *co1 co2* in Kronos in our study (Figure 5F) were associated with the down
620 regulation of *VRN2* transcripts. Taken together, these results are consistent with *CO1* and *CO2*
621 being promoters of *VRN2* transcription in the temperate grasses, a role that is likely more
622 important during the fall than in the spring, when high expression of *VRN1* results in the
623 downregulation of both *CO1* and *VRN2*.

624 Photoperiod and vernalization genes converge on the regulation of *FT1*, whose transcript levels
625 are well correlated with heading time [11, 47]. Since *PPD1* is a critical LD transcriptional
626 promoter of *FT1* [12, 32], it was not surprising to see almost undetectable levels of *FT1* in the
627 *ppd1* mutant, which were correlated with low *VRN1* transcript levels and late heading time
628 (Figure 5D-E). The low transcript levels of *VRN1* in the *ppd1* mutant may have contributed to
629 the slight increase in *VRN2* transcript levels observed in this mutant (Figure 5F), because *VRN1*
630 is a known transcriptional repressor of *VRN2* in wheat [27, 48].

631 The high transcript levels of *VRN2* in the *ppd1* mutant indicates that *PPD1* is not required for
632 the LD expression of *VRN2* (Figure 5F). However, several observations suggest that *PPD1* has a
633 positive effect on *VRN2* transcription. First, *VRN2* transcripts are upregulated under SD in lines
634 carrying the *Ppd-D1a* allele but not in sister lines carrying the *Ppd-D1b* allele [49]. Second, a
635 positive correlation has been reported between *PPD1* and *VRN2* transcript levels in young winter
636 barley plants in spite of a positive correlation between *PPD1* and *VRN1* [11]. Finally, *PPD1* and
637 *VRN2* showed similar transcription profiles in Kronos wild-type (Figure 5C and F). However,

638 those similarities disappear in the *CO1* and *CO2* mutants, suggesting that the effect of *PPD1* on
639 *VRN2* is modulated by *CO1* and *CO2*.

640 To summarize the dynamics of these transcriptional interactions during the seasons, we propose
641 the following working model for winter wheats. In the fall, *PPD1*, *CO1* and *CO2* promote the
642 expression of *VRN2* in the leaves, which prevents flowering by repressing the transcriptional
643 induction of *FT1*. During the winter, the increase in *VRN1* expression results in the gradual
644 downregulation of both *VRN2* and *CO1*, which facilitates the promotion of *FT1* by *PPD1* and the
645 initiation of flowering in the spring.

646

647 **Protein-protein interactions add an additional level of regulation to wheat heading time**

648 In addition to the complex transcriptional interactions described above, the proteins encoded by
649 the photoperiod genes form an intricate network of protein-protein interactions that contribute an
650 additional layer of complexity to the photoperiodic regulation of heading time. In Arabidopsis,
651 the central photoperiod gene *CO* is regulated at the transcriptional and posttranscriptional level.
652 A complex transcriptional regulation is required to establish the presence of *CO* mRNA during
653 the evening of a long day, when light can stabilize the CO protein, resulting in the activation of
654 *FT* transcription [23].

655 Several PRR proteins promote flowering in Arabidopsis by interacting with and stabilizing the
656 CO protein during the day specifically under LD, and indirectly through their roles in the
657 circadian clock [50]. Mutations in *PRR* genes delay Arabidopsis flowering under LD but not
658 under SD (similar to *PPD1* in wheat), with double mutants showing a stronger delay [51]. The
659 late-flowering Arabidopsis *prr7* mutant can be complemented by rice *OsPRR37* [52], suggesting

660 some conserved functions in rice and Arabidopsis. In this study, we detected interactions
661 between wheat PPD1 full-length protein and both CO1 and CO2 in Y2H and validated the CO1-
662 PPD1 interactions by split-YFP (Figure 7). These results suggest that the interactions between
663 CO and PRRs likely precede the split between monocot and dicot plants.

664 In spite of these similarities, there are also important differences between the grass *PPD1/PRR37*
665 gene and the homologous *PRR* genes from Arabidopsis. The Arabidopsis *PRR* genes are part of
666 the circadian clock and their mutants affect the expression of circadian clock genes and their
667 multiple downstream targets. By contrast, the natural mutation in the barley photoperiod
668 insensitive *ppd-H1* allele did not affect diurnal or circadian cycling of barley clock genes [53].
669 This result suggests that after the duplication that generated *PRR37* and *PRR73* in the grasses,
670 which is independent of the Arabidopsis duplication that originated *PRR3* and *PRR7*,
671 *PRR37/PPD1* acquired a more specialized role in the photoperiodic response with a more limited
672 role in the circadian clock.

673 In addition to its interactions with the LD flowering promoter PPD1, CO1 and CO2 can form
674 heterodimers with the LD flowering repressor VRN2, which is also a member of the CCT
675 domain protein family [30]. We hypothesize that the interactions with VRN2 might be relevant
676 to *CO1* and *CO2* function because loss-of-function mutation in *ghd7/vrn2* result in reversals of
677 functional in *OsPRR37* (*Hd2*) [43] and *OsCO1* (*Hd1*) in rice [41, 42], and *SbCO1* in sorghum
678 [38]. In rice, GHD7 binds to the transcription-activating domain of OsCO1, probably weakening
679 or blocking the transcriptional activation of *Ehd1* and *Hd3a* [42]. We have initiated crosses
680 among Kronos lines with mutations in *vrn2* [26], *co1*, *co2*, and *ppd1* to test these interactions in
681 wheat.

682 Recent studies in rice showed that another CCT-domain protein, the NUCLEAR
683 TRANSCRIPTION FACTOR Y subunit B-11 (NF-YB11 = HEME ACTIVATOR PROTEIN or
684 HAP-3H = *Ghd8*) has large effects on heading time and significant genetic interactions with
685 *OsGHD7*, *OsCO1* and *OsPRR37* [43]. We have previously shown that in addition to interacting
686 with each other, CO2 and VRN2 interact with the same subset of eight NUCLEAR FACTOR-Y
687 (NF-Y) transcription factors (Figure 7E) [30], suggesting an additional functional connection
688 between these proteins. This connection through the NF-Y proteins seems to less extensive
689 between CO1 and VRN2, where only one shared NF-Y interactor has been identified so far
690 (Figure 7E) [30]. Members of the NF-Y family have been shown to be involved in the regulation
691 of flowering through interactions with CCT domain proteins CO and COL in other plant species
692 [54-56]. Using yeast-three-hybrid (Y3H) assays, we previously showed that VRN2 competes
693 with CO2 for interactions with the NF-Ys, and that mutations in three conserved arginine (R)
694 residues within the CCT domain of VRN2 reduce the strength of the protein interactions and
695 competition with CO2 [30]. Since these same mutations abolish or reduce VRN2 function as a
696 LD flowering repressor, we hypothesize that the protein-protein interactions involving VRN2-
697 CO2-NF-Y CCT domain could be relevant for their function [30].

698 Phytochromes PHYB and PHYC are involved in the transcriptional regulation by light of both
699 *PPD1/PRR37* and *VRN2* in wheat [15, 28], *Brachypodium* [57], rice [58] and sorghum [37]. In
700 addition, OsPHYA, OsPHYB and OsGI proteins have been shown to interact directly with
701 OsGHD7, regulating protein stability [59]. We observed similar interactions between VRN2 and
702 both PHYB and PHYC in wheat. These two phytochromes also showed Y2H interactions with
703 CO1 and CO2, but not PPD1 (Figure 7E and S5). Additional experiments will be required to test

704 if these phytochrome interactions can stabilize the VRN2, CO1 and CO2 proteins in wheat as
705 they stabilize GHD7 in rice [59] or CO in Arabidopsis [60].

706 In summary, we found that CO1 and CO2 proteins can physically interact with each other and
707 with both PPD1 (a central LD flowering promoter) and VRN2 (a central LD flowering
708 repressor), providing a physical link between these central photoperiodic proteins (Figure 7E).
709 Among the 15 pairwise interactions tested among PHYB, PHYC, PPD1, CO1, CO2 and VRN2
710 80% showed positive interactions in Y2H assays indicating a complex and dense network of
711 protein interactions. We hypothesize that this network of protein interactions provides an
712 additional layer of molecular mechanisms that result in the complex genetic interactions in
713 heading time detected in this study.

714

715 **Two interacting photoperiod pathways in grasses**

716 A central conclusion of our study is that *PPD1* can perceive the differences in photoperiod and
717 adjust heading time accordingly even in the absence of any functional copy of *CO1* or *CO2.*
718 Similarly, *CO1* can accelerate heading time under LD in the absence of a functional copy of
719 *PPD1*. This is also true in rice, where heading time differences between SD and LD are observed
720 for *OsCO1* alleles in *Osprr37* mutants, and for *OsPRR37* alleles in rice *Osco1* mutants [43].
721 These results suggest that grasses have either two photoperiod pathways, each of them capable of
722 perceiving the length of the day/night and of regulating heading time, or a single point of
723 perception of the differences in photoperiod upstream of *PPD1* and *CO1* (e.g. *ELF3*), which can
724 then transmit the signal to both genes.

725 Another important conclusion from our study and from previous studies in sorghum and rice [37,
726 41, 43], is that the *CO* and *PRR37/PPD1* photoperiod pathways are extensively interconnected.
727 Changes in the balance of these interactions seem to play a central role in the diversity of
728 photoperiod responses in grasses, as suggested by changes in function observed when
729 photoperiodic genes are swapped between LD and SD species or when the same genes are
730 expressed in different mutant backgrounds in its own species. We hypothesize that the complex
731 feedback transcriptional regulatory loops and transcriptional interactions among photoperiod
732 genes along with the intricate interactions among their encoded proteins contribute to the
733 complex genetic interactions in heading time observed in this study and to the diversity of
734 photoperiodic responses in grasses.

735

736 **Materials and methods**

737 **Plant materials**

738 The materials used in this study included the tetraploid wheat variety Kronos (*Triticum*
739 *turgidum* ssp. *durum*), which carries a functional and dominant *Vrn-A1* allele for spring growth
740 habit, a functional but recessive *vrn-B1* allele for winter growth habit, a functional *Vrn-B2* long
741 day repressor (*ZCCT-B2a* and *ZCCT-B2b* [26]), and the *Ppd-A1a* (photoperiod insensitive or PI)
742 allele that confers earlier flowering under short days resulting in a reduced photoperiodic
743 response. We also used in our study near-isogenic lines of Kronos carrying either the
744 photoperiod sensitive *Ppd-A1b* (PS) allele [18] or no functional alleles in the *PPD-A1* and *PPD-*
745 *B1* homeologs (*ppd1*) [19].

746 Using previously published wheat sequences for *CO1* [45] and *CO2* [39], and the Kronos
747 transcriptome [61] we identified the A and B coding sequences for *CO1* and *CO2* in Kronos and

748 deposited them in GenBank under accession numbers MT043302 (*CO-A1*), MT043303 (*CO-B1*),
749 MT043304 (*CO-A2*), MT043305 (*CO-B2*). We used those sequences to identify loss-of-function
750 mutations in *CO1* and *CO2* in the Kronos TILLING population [21, 22], which are described in
751 detail in the Results section. We then combined mutations in the A and B homeologs from each
752 gene to generate loss-of-function *co1* (henceforth *co1*) and *co2* mutants (henceforth *co2*). We
753 backcrossed the individual mutant lines with wild-type Kronos at least two times to reduce
754 background mutations and then combined all four homozygous mutations to produce a *co1 co2*
755 mutant (henceforth *co1 co2*). In addition to the wild type Kronos-PI, the four homozygous *Co1*
756 *Co2*, *co1 Co2*, *Co1 co2* and *co1 co2* allelic classes were generated in Kronos-PS and the *ppd1*
757 mutant. We were not able to recover the triple loss-of-function mutant *ppd1 co1 co2* from any of
758 the tested progenies.

759 **Phenotyping**

760 We stratified wheat grains at 4 °C for 2 d in the dark and after germination we planted them in
761 pots in the soil. We evaluated the mutant and control lines in growth chambers set to 22 °C
762 during daylight and 17 °C during dark periods. Lights were set to 260-300 µmol $m^{-2}$ $s^{-1}$ and
763 were on for 16 h in LD experiments and 8 h in short day (SD) experiments. We recorded
764 flowering time as the total time from planting in soil to full emergences of the spike from the
765 sheath. Spikes were threshed and total grain number counted per spike.

766 **Statistical analysis**

767 We compared heading time in different genotypes using one-way ANOVAs for single locus and
768 factorial ANOVAs for two or more loci. We tested homogeneity of variances using the Levene's
769 test and normality of residuals with the Shapiro–Wilks test. We transformed the data when

770 necessary to satisfy the ANOVA assumptions. We performed all statistical analyses using SAS
771 9.4 (SAS Institute). Error bars in all graphs are standard errors of the means (s.e.m.).

772 **Gene expression analysis**

773 To study the effect of *ppd1*, *co1* and *co2* mutant alleles on the transcription profiles of genes
774 affecting wheat flowering, we collected leaves from plants grown in a CONVIRON growth
775 chamber with metal halide bulbs supplemented by florescent bulbs (16 h light / 8 h darkness, 22
776 °C day temperature and 17 °C night temperature, 300 µmol $m^{-2}$ $s^{-1}$). For the time course
777 experiment, we collected samples in liquid nitrogen every 4 h throughout the day from the newly
778 expanded fourth leaf. In this experiment, we included the *ppd1* mutant and all four possible
779 combinations of the *CO1* and *CO2* wild type and mutant alleles in the Kronos-PS (*Ppd-A1b*)
780 background.

781 RNA was isolated from leaves using the Spectrum Plant Total RNA Kit (Sigma-Aldrich)
782 following the manufacturer's recommendations. We treated the RNA samples with DNase
783 (Promega) according to the manufacturer's protocol prior to first-strand cDNA synthesis. We
784 assessed RNA integrity by a combination of A260/A280 and A260/A230 measurements and
785 running samples on a denaturing formaldehyde-agarose gel as recommended in the Qiagen
786 RNAeasy Mini Handbook. We used only samples with 260/280 and 260/230 ratios > 1.7 and no
787 degradation. We synthesized cDNA using 2.0 µg of total RNA per sample and M-MLV Reverse
788 Transcriptase (Promega) and poly-T primers (Sigma-Aldrich).

789 We performed the quantitative reverse transcription-PCR (qRT-PCR) assays using SybrGreen
790 Takara Master Mix in a 7500 Fast Real-Time PCR system (Applied Biosystems). For PCR, we
791 used one cycle at 95°C for 30 s and 40 cycles of 95°C for 5 s, 60°C for 5 s, and 72°C for 34 s,

792 followed by a melting curve program. We quantified expression using the delta Ct method ($2^{-}$
793 $^{\Delta CT}$) with *ACTIN* as endogenous control [15]. Primer efficiencies were all > 95% and their
794 sequences are summarized in Table S5. Primer sequences were previously described for *FT1* and
795 *VRN1* [47], *PPD1* [45], *CO1* and *CO2* [15] and *VRN2* [26].

796 **Yeast-two-hybrid (Y2H) and split yellow fluorescent protein (YFP) assays**

797 The full-length coding region of PPD1 was amplified from Kronos and the PHYB truncations
798 were amplified from *Triticum monococcum* with primers listed in Supplementary Table S5. The
799 amplified fragments were cloned into yeast vectors pGBKT7 and pGADT7 (Clontech,
800 http://www.clontech.com/), which were used to transform yeast strain Y2HGold (Clontech)
801 using the lithium acetate method. Transformants were selected on SD medium lacking leucine
802 (L) and tryptophan (W) plates and re-plated on SD medium lacking L, W, histidine (H) and
803 adenine (A) to test the interactions. Yeast vectors for VRN2 (full-length, both bait and prey),
804 CO1 (prey, including both B-boxes and CCT domain, amino acids 10 to 379) and CO2 (prey,
805 including both B-boxes and CCT domain, 15 to 356 amino acids) were previously described in
806 [30], and those for PHYC (N-PHYC, C-PHYC and FL-PHYC) and full-length PHYB (as prey)
807 in [15]. CO1 and CO2 showed strong auto-activation when used as baits so they were only used
808 as preys. The full-length PHYB gave strong autoactivation when used as bait, so we generated
809 two additional truncations N-PHYB and C-PHYB (primers in Table S5). Only N-PHYB can be
810 used as bait without autoactivation, and all three (N-PHYB, C-PHYB and FL-PHYB) can be
811 used as preys in Y2H assays. The truncated versions of PHYC include amino acids 1–600 (N-
812 terminal) and 601-1139 (C-terminal) [15], and those for PHYB amino acids (1-625 (N-terminal)
813 and 626-1166 (C-terminal).

814 For the bi-molecular fluorescent complementation (BiFC or split YFP) assays, each set of wheat
815 proteins was recombined into modified Gateway-compatible pY736 and pY735 which contain
816 the *UBIQUITIN* promoter to generate YFP-N-terminal fragment and YFP-C-terminal-fragment
817 fusion proteins. Wheat protoplasts were prepared, transfected and visualized as described in [62]

818

819 **ACKNOWLEDEMENTS**

820 This project was supported by NRI Competitive Grants 2017-67007-25939 and 2016-67013-
821 24617 from the USDA National Institute of Food and Agriculture (NIFA) and by the Howard
822 Hughes Medical Institute. Daniel Woods is a Howard Hughes Medical Institute Fellow of the
823 Life Sciences Research Foundation.

824

825 **AUTHOR CONTRIBUTIONS**

826 Lindsay M. Shaw: Investigation, Writing - Original Draft -Review & Editing. Chengxia Li:
827 Investigation, Writing - Original Draft -Review & Editing. Daniel Woods: Investigation, Writing
828 -Review & Editing. Maria A. Alvarez: Investigation, Writing -Review & Editing. Huiqiong:
829 Investigation, Methodology, Writing -Review & Editing. Mei Yee Lau: Investigation. Andrew
830 Chen: Investigation, Writing -Review & Editing. Jorge Dubcovsky: Conceptualization, Formal
831 analysis, Supervision, Project administration and funding acquisition, Writing –extensive Review
832 & Editing.

833

834 **CONFLICT OF INTEREST**

835 The authors declare that they do not have any conflict of interest.

836

837 **REFERENCES**


838 1. Bouche F, Woods DP, Amasino RM. Winter memory throughout the plant kingdom:
839 different paths to flowering. Plant Physiol. 2017;173(1):27-35. doi: 10.1104/pp.16.01322.
840 PMID: 27756819.
841 2. Garner WW, Allard HA. Effect of the relative length of day and night and other factors of
842 the environment on growth and reproduction in plants. J Agric Res. 1919;18:0553-606.
843 PMID: WOS:000188347200038.
844 3. Andres F, Coupland G. The genetic basis of flowering responses to seasonal cues. Nat
845 Rev Genet. 2012;13(9):627-39. doi: 10.1038/nrg3291. PMID: 22898651.
846 4. Suarez-Lopez P, Wheatley K, Robson F, Onouchi H, Valverde F, Coupland G.
847 CONSTANS mediates between the circadian clock and the control of flowering in
848 Arabidopsis. Nature. 2001;410(6832):1116-20. doi: 10.1038/35074138. PMID:
849 11323677.
850 5. Yanovsky MJ, Kay SA. Molecular basis of seasonal time measurement in Arabidopsis.
851 Nature. 2002;419(6904):308-12. doi: 10.1038/nature00996. PMID: 12239570.
852 6. Putterill J, Robson F, Lee K, Simon R, Coupland G. The CONSTANS gene of
853 Arabidopsis promotes flowering and encodes a protein showing similarities to zinc finger
854 transcription factors. Cell. 1995;80(6):847-57. doi: 10.1016/0092-8674(95)90288-0.
855 PMID: 7697715.
856 7. Griffiths S, Dunford RP, Coupland G, Laurie DA. The evolution of *CONSTANS*-like
857 gene families in barley, rice, and Arabidopsis. Plant Physiol. 2003;131(4):1855-67. doi:
858 10.1104/pp.102.016188. PMID: 12692345.

859 8. Yano M, Katayose Y, Ashikari M, Yamanouchi U, Monna L, Fuse T, et al. Hd1, a major
860 photoperiod sensitivity quantitative trait locus in rice, is closely related to the Arabidopsis
861 flowering time gene CONSTANS. Plant Cell. 2000;12(12):2473-84. doi:
862 10.1105/tpc.12.12.2473. PMID: 11148291.
863 9. Higgins JA, Bailey PC, Laurie DA. Comparative genomics of flowering time pathways
864 using *Brachypodium distachyon* as a model for the temperate grasses. PLoS One.
865 2010;5(4):e10065. doi: 10.1371/journal.pone.0010065. PMID: 20419097.
866 10. Campoli C, Drosse B, Searle I, Coupland G, von Korff M. Functional characterisation of
867 *HvCO1*, the barley (*Hordeum vulgare*) flowering time ortholog of *CONSTANS*. Plant J.
868 2012;69(5):868-80. doi: 10.1111/j.1365-313X.2011.04839.x. PMID: 22040323.
869 11. Mulki MA, von Korff M. CONSTANS controls floral repression by up-regulating
870 *VERNALIZATION2* (*VRN-H2*) in Barley. Plant Physiol. 2016;170(1):325-37. doi:
871 10.1104/pp.15.01350. PMID: 26556793.
872 12. Turner A, Beales J, Faure S, Dunford RP, Laurie DA. The pseudo-response regulator
873 *Ppd-H1* provides adaptation to photoperiod in barley. Science. 2005;310(5750):1031-4.
874 doi: 10.1126/science.1117619. PMID: 16284181.
875 13. Koo BH, Yoo SC, Park JW, Kwon CT, Lee BD, An G, et al. Natural variation in
876 *OsPRR37* regulates heading date and contributes to rice cultivation at a wide range of
877 latitudes. Mol Plant. 2013;6(6):1877-88. doi: 10.1093/mp/sst088. PMID: 23713079.
878 14. Murphy RL, Klein RR, Morishige DT, Brady JA, Rooney WL, Miller FR, et al.
879 Coincident light and clock regulation of pseudoresponse regulator protein 37 (PRR37)
880 controls photoperiodic flowering in sorghum. Proc Natl Acad Sci U S A.
881 2011;108(39):16469-74. doi: 10.1073/pnas.1106212108. PMID: 21930910.

882 15. Chen A, Li C, Hu W, Lau MY, Lin H, Rockwell NC, et al. Phytochrome C plays a major
883 role in the acceleration of wheat flowering under long-day photoperiod. Proc Natl Acad
884 Sci U S A. 2014;111(28):10037-44. doi: 10.1073/pnas.1409795111. PMID: 24961368.
885 16. Beales J, Turner A, Griffiths S, Snape JW, Laurie DA. A pseudo-response regulator is
886 misexpressed in the photoperiod insensitive Ppd-D1a mutant of wheat (Triticum aestivum
887 L.). Theor Appl Genet. 2007;115(5):721-33. doi: 10.1007/s00122-007-0603-4. PMID:
888 17634915.
889 17. Wilhelm EP, Turner AS, Laurie DA. Photoperiod insensitive *Ppd-A1a* mutations in
890 tetraploid wheat (*Triticum durum* Desf.). Theor Appl Genet. 2009;118(2):285-94. doi:
891 10.1007/s00122-008-0898-9. PMID: 18839130.
892 18. Pearce S, Vanzetti LS, Dubcovsky J. Exogenous gibberellins induce wheat spike
893 development under short days only in the presence of *VERNALIZATION1*. Plant Physiol.
894 2013;163(3):1433-45. doi: 10.1104/pp.113.225854. PMID: 24085801.
895 19. Pearce S, Shaw LM, Lin H, Cotter JD, Li C, Dubcovsky J. Night-break experiments shed
896 light on the *Photoperiod1*-mediated flowering. Plant Physiol. 2017;174(2):1139-50. doi:
897 10.1104/pp.17.00361. PMID: 28408541.
898 20. Shaw LM, Turner AS, Herry L, Griffiths S, Laurie DA. Mutant alleles of *Photoperiod-1*
899 in wheat (*Triticum aestivum* L.) that confer a late flowering phenotype in long days.
900 PLoS One. 2013;8(11):e79459. doi: 10.1371/journal.pone.0079459. PMID: 24244507.
901 21. Krasileva KV, Vasquez-Gross HA, Howell T, Bailey P, Paraiso F, Clissold L, et al.
902 Uncovering hidden variation in polyploid wheat. Proc Natl Acad Sci U S A.
903 2017;114(6):E913-E21. doi: 10.1073/pnas.1619268114. PMID: 28096351.

904 22. Uauy C, Paraiso F, Colasuonno P, Tran RK, Tsai H, Berardi S, et al. A modified
905 TILLING approach to detect induced mutations in tetraploid and hexaploid wheat. BMC
906 Plant Biol. 2009;9:115. doi: 10.1186/1471-2229-9-115. PMID: 19712486.
907 23. Valverde F. CONSTANS and the evolutionary origin of photoperiodic timing of
908 flowering. J Exp Bot. 2011;62(8):2453-63. doi: 10.1093/jxb/erq449. PMID: 21239381.
909 24. Waddington SR, Cartwright PM, Wall PC. A quantitative scale of spike initial and pistil
910 development in barley and wheat. Ann Bot-London. 1983;51(1):119-30. PMID:
911 WOS:A1983QC01200013.
912 25. Alvarez MA, Tranquilli G, Lewis S, Kippes N, Dubcovsky J. Genetic and physical
913 mapping of the earliness *per se* locus *Eps-A*$^{m}$*1* in *Triticum monococcum* identifies *EARLY*
914 *FLOWERING 3* (*ELF3*) as a candidate gene. Funct Integr Genomic. 2016;16(4):365-82.
915 doi: 10.1007/s10142-016-0490-3. PMID: 27085709.
916 26. Distelfeld A, Tranquilli G, Li C, Yan L, Dubcovsky J. Genetic and molecular
917 characterization of the *VRN2* loci in tetraploid wheat. Plant Physiol. 2009;149(1):245-57.
918 doi: 10.1104/pp.108.129353. PMID: 19005084.
919 27. Chen A, Dubcovsky J. Wheat TILLING mutants show that the vernalization gene *VRN1*
920 down-regulates the flowering repressor *VRN2* in leaves but is not essential for flowering.
921 PLoS Genet. 2012;8(12):e1003134. doi: 10.1371/journal.pgen.1003134. PMID:
922 23271982.
923 28. Pearce S, Kippes N, Chen A, Debernardi JM, Dubcovsky J. RNA-seq studies using wheat
924 *PHYTOCHROME B* and *PHYTOCHROME C* mutants reveal shared and specific
925 functions in the regulation of flowering and shade-avoidance pathways. BMC Plant Biol.
926 2016;16(1):141. doi: 10.1186/s12870-016-0831-3. PMID: 27329140.

927 29. Kippes N, van Gessel C, Hamilton J, Akpinar A, Budak H, Dubcovsky J, et al. Effect of
928 *phyB* and *phyC* loss-of-function mutations on wheat transcriptome under short and long
929 day photoperiods. bioRxiv. 2020. doi: https://doi.org/10.1101/2020.04.07.030197.
930 30. Li C, Distelfeld A, Comis A, Dubcovsky J. Wheat flowering repressor VRN2 and
931 promoter CO2 compete for interactions with NUCLEAR FACTOR-Y complexes. Plant J.
932 2011;67(5):763-73. doi: 10.1111/j.1365-313X.2011.04630.x. PMID: 21554456.
933 31. Faure S, Turner AS, Gruszka D, Christodoulou V, Davis SJ, von Korff M, et al. Mutation
934 at the circadian clock gene *EARLY MATURITY 8* adapts domesticated barley (*Hordeum*
935 *vulgare*) to short growing seasons. Proc Natl Acad Sci U S A. 2012;109(21):8328-33.
936 doi: 10.1073/pnas.1120496109. PMID: 22566625.
937 32. Gao M, Geng F, Klose C, Staudt A-M, Huang H, Nguyen D, et al. Phytochromes
938 measure photoperiod in *Brachypodium*. bioRxiv. 2019. doi: 10.1101/697169.
939 33. Diaz A, Zikhali M, Turner AS, Isaac P, Laurie DA. Copy number variation affecting the
940 *Photoperiod-B1* and *Vernalization-A1* genes is associated with altered flowering time in
941 wheat (*Triticum aestivum*). PLoS One. 2012;7(3):e33234. doi:
942 10.1371/journal.pone.0033234. PMID: 22457747.
943 34. Stracke S, Haseneyer G, Veyrieras JB, Geiger HH, Sauer S, Graner A, et al. Association
944 mapping reveals gene action and interactions in the determination of flowering time in
945 barley. Theor Appl Genet. 2009;118(2):259-73. doi: 10.1007/s00122-008-0896-y. PMID:
946 18830577.
947 35. Alqudah AM, Sharma R, Pasam RK, Graner A, Kilian B, Schnurbusch T. Genetic
948 dissection of photoperiod response based on GWAS of pre-anthesis phase duration in

949 spring barley. PLoS One. 2014;9(11):e113120. doi: 10.1371/journal.pone.0113120.
950 PMID: 25420105.
951 36. Casto AL, Mattison AJ, Olson SN, Thakran M, Rooney WL, Mullet JE. *Maturity2*, a
952 novel regulator of flowering time in *Sorghum bicolor*, increases expression of *SbPRR37*
953 and *SbCO* in long days delaying flowering. PLoS One. 2019;14(4):e0212154. doi:
954 10.1371/journal.pone.0212154. PMID: 30969968.
955 37. Yang S, Murphy RL, Morishige DT, Klein PE, Rooney WL, Mullet JE. Sorghum
956 phytochrome B inhibits flowering in long days by activating expression of *SbPRR37* and
957 *SbGHD7*, repressors of *SbEHD1*, *SbCN8* and *SbCN12*. PLoS One. 2014;9(8):e105352.
958 doi: 10.1371/journal.pone.0105352. PMID: 25122453.
959 38. Yang S, Weers BD, Morishige DT, Mullet JE. *CONSTANS* is a photoperiod regulated
960 activator of flowering in sorghum. BMC Plant Biol. 2014;14:148. doi: 10.1186/1471-
961 2229-14-148. PMID: 24884377.
962 39. Nemoto Y, Kisaka M, Fuse T, Yano M, Ogihara Y. Characterization and functional
963 analysis of three wheat genes with homology to the *CONSTANS* flowering time gene in
964 transgenic rice. Plant J. 2003;36(1):82-93. doi: 10.1046/j.1365-313x.2003.01859.x.
965 PMID: 12974813.
966 40. Woods DP, McKeown MA, Dong Y, Preston JC, Amasino RM. Evolution of
967 *VRN2/Ghd7*-like genes in vernalization-mediated repression of grass flowering. Plant
968 Physiol. 2016;170(4):2124-35. doi: 10.1104/pp.15.01279. PMID: 26848096.
969 41. Fujino K, Yamanouchi U, Nonoue Y, Obara M, Yano M. Switching genetic effects of the
970 flowering time gene *Hd*1 in LD conditions by *Ghd7* and *OsPRR37* in rice. Breeding Sci.
971 2019;69(1):127-32. doi: 10.1270/jsbbs.18060. PMID: 31086490.

972 42. Zhang Z, Hu W, Shen G, Liu H, Hu Y, Zhou X, et al. Alternative functions of Hd1 in
973 repressing or promoting heading are determined by Ghd7 status under long-day
974 conditions. Sci Rep-Uk. 2017;7(1):5388. doi: 10.1038/s41598-017-05873-1. PMID:
975 28710485.
976 43. Zhang B, Liu H, Qi F, Zhang Z, Li Q, Han Z, et al. Genetic interactions among *Ghd7*,
977 *Ghd8*, *OsPRR37* and *Hd1* contribute to large variation in heading date in rice. Rice (N
978 Y). 2019;12(1):48. doi: 10.1186/s12284-019-0314-x. PMID: 31309345.
979 44. Maurer A, Draba V, Jiang Y, Schnaithmann F, Sharma R, Schumann E, et al. Modelling
980 the genetic architecture of flowering time control in barley through nested association
981 mapping. BMC Genomics. 2015;16:290. doi: 10.1186/s12864-015-1459-7. PMID:
982 25887319.
983 45. Shaw LM, Turner AS, Laurie DA. The impact of photoperiod insensitive *Ppd-1a*
984 mutations on the photoperiod pathway across the three genomes of hexaploid wheat
985 (*Triticum aestivum*). Plant J. 2012;71(1):71-84. doi: 10.1111/j.1365-313X.2012.04971.x.
986 PMID: 22372488.
987 46. Qin Z, Bai Y, Muhammad S, Wu X, Deng P, Wu J, et al. Divergent roles of *FT-like 9* in
988 flowering transition under different day lengths in *Brachypodium distachyon*. Nat
989 Commun. 2019;10(1):812. doi: 10.1038/s41467-019-08785-y. PMID: 30778068.
990 47. Yan L, Fu D, Li C, Blechl A, Tranquilli G, Bonafede M, et al. The wheat and barley
991 vernalization gene *VRN3* is an orthologue of *FT*. Proc Natl Acad Sci U S A.
992 2006;103(51):19581-6. doi: 10.1073/pnas.0607142103. PMID: 17158798.

993 48. Deng W, Casao MC, Wang P, Sato K, Hayes PM, Finnegan EJ, et al. Direct links
994 between the vernalization response and other key traits of cereal crops. Nat Commun.
995 2015;6:5882. doi: 10.1038/ncomms6882. PMID: 25562483.
996 49. Turner AS, Faure S, Zhang Y, Laurie DA. The effect of day-neutral mutations in barley
997 and wheat on the interaction between photoperiod and vernalization. Theor Appl Genet.
998 2013;126(9):2267-77. doi: 10.1007/s00122-013-2133-6. PMID: 23737074.
999 50. Hayama R, Sarid-Krebs L, Richter R, Fernandez V, Jang S, Coupland G. PSEUDO
1000 RESPONSE REGULATORs stabilize CONSTANS protein to promote flowering in
1001 response to day length. Embo J. 2017;36(7):904-18. doi: 10.15252/embj.201693907.
1002 PMID: 28270524.
1003 51. Nakamichi N, Kita M, Ito S, Yamashino T, Mizuno T. PSEUDO-RESPONSE
1004 REGULATORS, PRR9, PRR7 and PRR5, together play essential roles close to the
1005 circadian clock of *Arabidopsis thaliana*. Plant Cell Physiol. 2005;46(5):686-98. doi:
1006 10.1093/pcp/pci086. PMID: 15767265.
1007 52. Murakami M, Tago Y, Yamashino T, Mizuno T. Characterization of the rice circadian
1008 clock-associated pseudo-response regulators in *Arabidopsis thaliana*. Biosci Biotech
1009 Bioch. 2007;71(4):1107-10. doi: 10.1271/bbb.70048. PMID: 17420570.
1010 53. Campoli C, Shtaya M, Davis SJ, von Korff M. Expression conservation within the
1011 circadian clock of a monocot: natural variation at barley *Ppd-H1* affects circadian
1012 expression of flowering time genes, but not clock orthologs. BMC Plant Biol.
1013 2012;12:97. doi: 10.1186/1471-2229-12-97. PMID: 22720803.
1014 54. Ben-Naim O, Eshed R, Parnis A, Teper-Bamnolker P, Shalit A, Coupland G, et al. The
1015 CCAAT binding factor can mediate interactions between CONSTANS-like proteins and

1016 DNA. Plant J. 2006;46(3):462-76. doi: 10.1111/j.1365-313X.2006.02706.x. PMID:
1017 16623906.
1018 55. Kumimoto RW, Adam L, Hymus GJ, Repetti PP, Reuber TL, Marion CM, et al. The
1019 Nuclear Factor Y subunits NF-YB2 and NF-YB3 play additive roles in the promotion of
1020 flowering by inductive long-day photoperiods in Arabidopsis. Planta. 2008;228(5):709-
1021 23. doi: 10.1007/s00425-008-0773-6. PMID: 18600346.
1022 56. Wenkel S, Turck F, Singer K, Gissot L, Le Gourrierec J, Samach A, et al. CONSTANS
1023 and the CCAAT box binding complex share a functionally important domain and interact
1024 to regulate flowering of Arabidopsis. Plant Cell. 2006;18(11):2971-84. doi:
1025 10.1105/tpc.106.043299. PMID: 17138697.
1026 57. Woods DP, Ream TS, Minevich G, Hobert O, Amasino RM. PHYTOCHROME C is an
1027 essential light receptor for photoperiodic flowering in the temperate grass, *Brachypodium*
1028 *distachyon*. Genetics. 2014;198(1):397-408. doi: 10.1534/genetics.114.166785. PMID:
1029 25023399.
1030 58. Osugi A, Itoh H, Ikeda-Kawakatsu K, Takano M, Izawa T. Molecular dissection of the
1031 roles of phytochrome in photoperiodic flowering in rice. Plant Physiol.
1032 2011;157(3):1128-37. doi: 10.1104/pp.111.181792. PMID: 21880933.
1033 59. Zheng T, Sun J, Zhou S, Chen S, Lu J, Cui S, et al. Post-transcriptional regulation of
1034 Ghd7 protein stability by phytochrome and OsGI in photoperiodic control of flowering in
1035 rice. New Phytol. 2019;224(1):306-20. doi: 10.1111/nph.16010. PMID: 31225911.
1036 60. Valverde F, Mouradov A, Soppe W, Ravenscroft D, Samach A, Coupland G.
1037 Photoreceptor regulation of CONSTANS protein in photoperiodic flowering. Science.
1038 2004;303(5660):1003-6. doi: 10.1126/science.1091761. PMID: 14963328.

1039 61. Krasileva KV, Buffalo V, Bailey P, Pearce S, Ayling S, Tabbita F, et al. Separating
1040 homeologs by phasing in the tetraploid wheat transcriptome. Genome Biol.
1041 2013;14(6):R66. doi: 10.1186/gb-2013-14-6-r66. PMID: 23800085.
1042 62. Shan Q, Wang Y, Li J, Gao C. Genome editing in rice and wheat using the CRISPR/Cas
1043 system. Nat Protoc. 2014;9(10):2395-410. doi: 10.1038/nprot.2014.157. PMID:
1044 25232936.

1045

1046

1047 **SUPPORTING INFORMATION CAPTIONS**

1048 **Supplementary Figure S1.** Shoot apical meristem (SAM) and spike development.

1049 **Supplementary Figure S2.** Dissection of developing spikes.

1050 **Supplementary Figure S3.** Effect of *ppd1*, *co1* and *co2* loss-of-function mutations and
1051 photoperiod on *CO1* and *CO2* transcript levels.

1052 **Supplementary Figure S4.** Effect of *phyB*-null and *phyC*-null mutations in Kronos-PI on the
1053 transcriptional profiles of *CO1* and *CO2* under SD and LD.

1054 **Supplementary Figure S5.** Yeast-two-hybrid (Y2H) assays.

1055 **Supplementary Table S1.** Genome-specific primer sequences and PCR conditions for
1056 TILLING.

1057 **Supplementary Table S2.** Number of mutations detected in the targeted regions of wheat *CO1*
1058 and *CO2* homologs in the Kronos TILLING population.

1059 **Table S3**. Analysis of variance for heading time under long days.

1060 **Table S4**. Analysis of variance for heading time under short days.

1061 **Table S5**. Primers used in the qRT-PCR and Y2H experiments.